Atmos. Meas. Tech., 9, 2909–2925, 2016
www.atmos-meas-tech.net/9/2909/2016/
doi:10.5194/amt-9-2909-2016

Atmospheric Measurement Techniques
Open Access
EGU

Evaluation of NO^+ reagent ion chemistry for online measurements of atmospheric volatile organic compounds

Abigail R. Koss[1,2,3], Carsten Warneke[1,2], Bin Yuan[1,2], Matthew M. Coggon[1,2], Patrick R. Veres[1,2], and Joost A. de Gouw[1,2,3]

[1]NOAA Earth System Research Laboratory (ESRL), Chemical Sciences Division, Boulder, CO, USA
[2]Cooperative Institute for Research in Environmental Sciences, University of Colorado at Boulder, Boulder, CO, USA
[3]Department of Chemistry and Biochemistry, University of Colorado at Boulder, CO, USA

Correspondence to: Abigail R. Koss (abigail.koss@noaa.gov)

Received: 9 March 2016 – Published in Atmos. Meas. Tech. Discuss.: 7 April 2016
Revised: 18 June 2016 – Accepted: 21 June 2016 – Published: 8 July 2016

Abstract. NO^+ chemical ionization mass spectrometry (NO^+ CIMS) can achieve fast (1 Hz and faster) online measurement of trace atmospheric volatile organic compounds (VOCs) that cannot be ionized with H_3O^+ ions (e.g., in a PTR-MS or H_3O^+ CIMS instrument). Here we describe the adaptation of a high-resolution time-of-flight H_3O^+ CIMS instrument to use NO^+ primary ion chemistry. We evaluate the NO^+ technique with respect to compound specificity, sensitivity, and VOC species measured compared to H_3O^+. The evaluation is established by a series of experiments including laboratory investigation using a gas-chromatography (GC) interface, in situ measurement of urban air using a GC interface, and direct in situ measurement of urban air. The main findings are that (1) NO^+ is useful for isomerically resolved measurements of carbonyl species; (2) NO^+ can achieve sensitive detection of small (C_4–C_8) branched alkanes but is not unambiguous for most; and (3) compound-specific measurement of some alkanes, especially isopentane, methylpentane, and high-mass (C_{12}–C_{15}) n-alkanes, is possible with NO^+. We also demonstrate fast in situ chemically specific measurements of C_{12} to C_{15} alkanes in ambient air.

1 Introduction

Volatile organic compounds (VOCs) are central to the formation of ozone and secondary organic aerosol and can have direct human health effects. Attempting to understand the behavior of these species in the troposphere presents several measurement challenges (Glasius and Goldstein, 2016). First, VOCs are highly chemically diverse. Second, many environmentally important species require measurement precision of better than 100 parts per trillion (ppt). Finally, numerous applications, such as eddy flux analyses or sampling from a mobile platform, require fast in situ measurements, with 1 min or faster time resolution.

H_3O^+ chemical ionization mass spectrometry (H_3O^+ CIMS), more commonly known as proton-transfer-reaction mass spectrometry (PTR-MS), is a well-established approach to measuring VOCs (de Gouw and Warneke, 2007; Jordan et al., 2009b). In H_3O^+ CIMS, air is mixed with hydronium (H_3O^+) ions in a drift tube region. VOCs are ionized by transfer of the proton from H_3O^+ to the VOC. These instruments are capable of VOC measurements that are fast, sensitive, and chemically detailed (Jordan et al., 2009b; Graus et al., 2010; Sulzer et al., 2014; Yuan et al., 2016).

Despite these advantages, H_3O^+ CIMS has several limitations related to the reagent ion chemistry. For one, this technique generally cannot distinguish between isomers. For instance, this is a significant limitation when measuring aldehyde and ketone carbonyl isomers, which display very different behavior in the atmosphere. Separation of propanal and acetone with PTR-MS has been explored using collision-induced dissociation with an ion-trap mass analyzer, but this technique negatively affects the instrument time resolution and sensitivity (Warneke et al., 2005). Additionally, some proton transfer reactions are dissociative. Large hydrocarbons (C_8 and larger) fragment into common small masses, making spectra difficult to interpret (Jobson et al., 2005; Er-

ickson et al., 2014; Gueneron et al., 2015). Alcohols and aldehydes can lose H_2O, lowering the sensitivity to the protonated parent mass; their product ion masses then coincide with those of hydrocarbons, making independent measurement difficult (Španěl et al., 1997; Buhr et al., 2002). Furthermore, H_3O^+ CIMS is not sensitive to small ($\sim C_8$ and smaller) saturated alkanes, as their proton affinities are lower than or very close to that of water (Arnold et al., 1998; Gueneron et al., 2015). This is a serious limitation in studies of urban air or emissions from oil and natural gas extractions, where small alkanes can contribute a large fraction to the total gas phase carbon and chemical reactivity (Katzenstein et al., 2003; Gilman et al., 2013). Gas-chromatography (GC) techniques avoid many of these limitations but have much slower time resolution.

Use of NO^+ reagent ion chemistry may address some of the limitations of H_3O^+. Reaction of NO^+ with various VOCs has been extensively studied using selected-ion flow tube methods (SIFT-MS). SIFT methods use a quadrupole mass filter between the ion source and ion–molecule reactor, which provides a very pure reagent ion source but limits the primary ion signal. SIFT studies have identified the major products of the reaction of NO^+ with VOCs representative of many different functional groups (Španěl and Smith, 1996, 1998a, b, 1999; Španěl et al., 1997; Arnold et al., 1998; Francis et al., 2007a, b). Aldehydes and ketones are easily separable: ketones cluster with NO^+, forming mass $(m+30)$ ions, whereas aldehydes react by hydride abstraction, forming mass $(m-1)$ ions (where m is the molecular mass of the species). Rather than losing H_2O, as in H_3O^+ CIMS, alcohols react by NO^+ adduct formation or hydride abstraction. And finally, NO^+ can be used to detect alkanes: small ($>C_4$) branched alkanes and large ($>C_8$) n-alkanes react by hydride abstraction, forming mass $(m-1)$.

The application of SIFT methods to atmospheric analysis has been limited by relatively poor sensitivity (Smith and Španěl, 2005; Francis et al., 2007b; de Gouw and Warneke, 2007), although better sensitivities have been reported in recent years (Prince et al., 2010). The adaptation of an existing CIMS instrument to use the SIFT technique requires extensive instrument modification or the purchase of an external SIFT unit (Karl et al., 2012). Several groups have experimented with low-cost adaptation of H_3O^+ CIMS instruments to use NO^+ chemistry. Knighton et al. (2009) adapted an H_3O^+ CIMS instrument to measure 1,3-butadiene and demonstrated in situ detection of this species in the atmosphere. Jordan et al. (2009a) have developed a hollow-cathode ion source capable of switchable reagent ion chemistry, and they demonstrated laboratory measurement with NO^+ of several aromatics, chlorinated aromatics, and carbonyls, with sensitivities comparable to H_3O^+ CIMS. The NO^+ capability of the Jordan et al. instrument has been used in the laboratory by Inomata et al. (2013) to investigate detection of n-tridecane, by Agarwal et al. (2014) to measure picric acid, and by Liu et al. (2013) to investigate the behavior of methyl vinyl ketone (MVK) and methacrolein in a reaction chamber.

These studies suggest that an easy, low-cost adaptation of H_3O^+ CIMS instruments to NO^+ chemistry could greatly enhance our capability to measure VOCs in the atmosphere. However, the number of VOC species investigated to date is small and few field measurements have been reported. The ability of a modified H_3O^+ CIMS instrument to separate carbonyl isomers in ambient air, and to measure small alkanes both in the laboratory and in ambient air, has not been evaluated. Finally, the lack of fragmentation of n-tridecane reported in Inomata et al. (2013) is intriguing, but the use of an NO^+ CIMS instrument to measure similar high-mass alkanes in ambient air has not been demonstrated.

Here we evaluate the adaptation of an H_3O^+ CIMS instrument to use NO^+ reagent ion chemistry. We provide specifics on instrument setup and operating parameters. We report the sensitivity and spectral simplicity of NO^+ CIMS, relative to H_3O^+ CIMS, for nearly 100 atmospherically relevant VOCs, including a wide range of functional groups, and provide product ion distributions for several representative compounds. We demonstrate, interpret, and evaluate measurements of separate aldehyde and ketone isomers, light alkanes, and several other species in ambient air. Finally, we investigate measurement of high-molecular-mass alkanes using NO^+. We extend the laboratory analysis of high-mass alkanes to C_{12}–C_{15} n-alkanes and demonstrate fast, in situ measurement of these species in ambient air.

2 Methods

2.1 Instrumentation

Two separate H_3O^+ CIMS instruments (referred to hereafter as PTR-QMS and H_3O^+ ToF-CIMS) were adapted to NO+ chemistry in this work. Both instruments consist of (1) a hollow cathode reagent ion source, (2) a drift tube reaction region, (3) an ion transfer stage that transports from the drift tube to the mass analyzer and allows differential pumping, and (4) a mass analyzer. Both instruments have nearly identical hollow cathode ion sources and drift tube reaction regions, described in detail in de Gouw and Warneke (2007). The PTR-QMS (Ionicon Analytik) uses ion lenses to transfer ions from the drift tube to a unit-mass-resolution quadrupole mass analyzer (Pfeiffer). This instrument is described further by de Gouw and Warneke (2007). The H_3O^+ ToF-CIMS uses RF-only segmented quadrupole ion guides to transfer ions from the drift tube to a time-of-flight mass analyzer produced by Aerodyne Research Inc./Tofwerk with a mass resolution of 4000–6000 (Bertram et al., 2011). This instrument is described further by Yuan et al. (2016). A similar PTR-ToF instrument using quadrupole ion guides has also been recently described (Sulzer et al., 2014). ToF-CIMS data were analyzed using Tofwerk high-resolution peak-fitting software

(Aerodyne Research Inc./Tofwerk AG). A description of the algorithm is given in DeCarlo et al. (2006).

A GC instrument was used both as an interface to the ToF-CIMS and as a separate instrument using an electron-impact quadrupole mass spectrometer. The GC collects VOCs in a liquid nitrogen cryotrap for a 5 min period every 30 min. VOCs are then injected onto parallel Al_2O_3/KCl PLOT and semi-polar DB-624 capillary columns to separate C_2–C_{11} hydrocarbons and heteroatom-containing VOCs. When used as an interface to the ToF-CIMS, the column eluant was directed to the inlet of the ToF-CIMS, where it was diluted with 50 sccm of clean air with controlled humidity. When operated as a separate instrument, the column eluant was directed to an electron-ionization quadrupole mass spectrometer (EIMS) operated in selected-ion mode. The response of this GC-EIMS instrument to various VOCs has been well characterized over a long period of field and laboratory applications, and further operational details have been reported elsewhere (Goldan et al., 2004; Gilman et al., 2010, 2013).

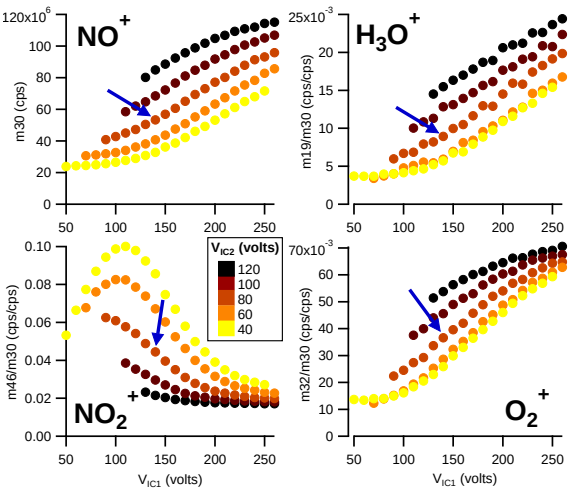

Figure 1. Dependence of NO^+, H_3O^+, NO_2^+, and O_2^+ on intermediate chamber voltages. The arrow denotes the selected operating conditions. Experiment conducted in dry air (H_3O^+ is from residual water in the instrument and in commercial ultra-zero air.)

2.2 Adaptation of H_3O^+ to NO^+ CIMS

Ideally, both H_3O^+ and NO^+ reagent ion chemistry can be utilized with a single instrument. The fewest possible number of hardware parameters were changed to facilitate fast switching and instrument stability.

To achieve generation of NO^+ ions, the water reservoir was replaced with ultra-high-purity air. The source gas flow (5 sccm), the hollow cathode parameters, and the drift tube operating pressure (2.4 mbar) were not changed. To optimize the generation of NO^+ ions relative to H_3O^+, O_2^+, and NO_2^+, and the generation of the desired VOC^+ ion products, the voltages of the intermediate chamber plates, V_{IC1} and V_{IC2}, and the drift tube voltage V_{DT} were adjusted. An instrument schematic showing the locations of V_{IC1}, V_{IC2}, and V_{DT} can be found in the Supplement (Fig. S1). Optimization was performed sampling dry air.

It has been demonstrated that the quadrupole ion guides of the ToF-CIMS can significantly change the measured distribution of reagent and impurity ions (Yuan et al., 2016). The PTR-QMS does not have that issue as strongly (modeled and measured cluster distributions are largely similar, as discussed by de Gouw and Warneke, 2007) and therefore we explored the effect of V_{IC1}, V_{IC2}, and V_{DT} on reagent ion distribution using the PTR-QMS. As the PTR-QMS and ToF-CIMS have nearly identical ion source and drift tube design, we assume that ion behavior in these regions is the same for the two instruments.

First, V_{DT} was held constant at 720 V (the original setting of the PTR-QMS instrument), and V_{IC1} and V_{IC2} were varied (Fig. 1). The settings of V_{IC1} (140 V) and V_{IC2} (80 V) were selected as a compromise between high NO^+ ion count rate and low-impurity ion count rates. The major impurity ions are H_3O^+, O_2^+, and NO_2^+, and it is desirable to limit the formation of these ions because they react with VOCs, complicating the interpretation of spectra. Next, several VOCs with different functional groups were introduced into the instrument, separately, and the drift tube electric potential scanned. A drift tube voltage of 350 V (electric field intensity relative to gas number density $E/N = 60$ Td) was selected as a compromise between maximizing NO^+ ion count rate, minimizing H_3O^+, O_2^+, and NO_2^+, maximizing VOC ion count rates, minimizing alkane fragmentation, and promoting different product ions for carbonyls and aldehydes (Fig. 2). This setting results in about 10×10^6 cps (counts per second) of NO^+ primary ions, while in typical PTR-MS settings we achieve about 30×10^6 cps of H_3O^+ primary ions.

We note that the E/N of 60 Td used for the NO^+ CIMS is much lower than that used in typical PTR-MS settings (circa 120 Td). In air, NO^+ will react with water to produce H_3O^+ and HNO_2 (Fehsenfeld et al., 1971). The electric field in the drift tube limits the formation of the $NO^+ \cdot (H_2O)_n$ intermediaries in this reaction, promoting high NO^+ count rates and VOC sensitivity. In PTR-MS, the drift field is used to prevent the formation of analogous $H_3O^+ \cdot (H_2O)_n$ clusters. The bond energy of $H_3O^+ \cdot (H_2O)_n$ clusters is significantly higher than that of $NO^+ \cdot (H_2O)_n$ clusters (Keesee and Castleman, 1986); hence the need for a higher E/N in PTR-MS settings.

The remainder of the work detailed in this paper was performed using the ToF-CIMS with the settings as described here. The ToF-CIMS has the advantages of high mass resolution, fast time resolution, and simultaneous measurement of all masses. Further small adjustments were made to the ToF-CIMS quadrupole ion guide voltages using Thuner software (Tofwerk AG) to promote sensitivity to VOCs and separate carbonyl isomers. The two most important such adjustments decreased the electric potentials immediately upstream of each quadrupole ion guide (Fig. S2). These adjustments re-

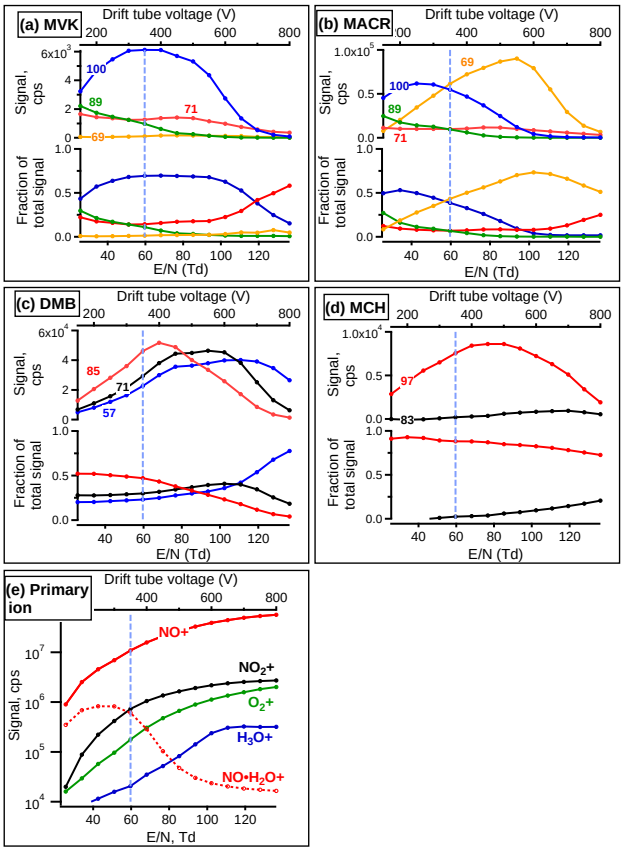

Figure 2. VOC and primary product ion dependence on drift tube voltage. Traces are labeled by the nominal product ion m/z in Th. **(a)** Methyl vinyl ketone; **(b)** methacrolein; **(c)** 2,2-dimethylbutane; **(d)** methylcyclohexane; **(e)** primary ions and clusters. The dashed line indicates the selected operating voltage. Experiment conducted in dry air (H_3O^+ is from residual water in the instrument and in commercial ultra-zero air.)

duced declustering at these locations, which improved the transmission of VOC $\cdot$ NO^+ clusters.

3 Results and discussion

3.1 Laboratory experiments

3.1.1 Sensitivity and simplicity of the NO^+ reagent ion chemistry

VOCs from several calibration cylinders (VOCs listed in Table S1 in the Supplement) were diluted with high purity air to mixing ratios of approximately 10 ppbv and introduced into the sampling inlet of the GC interface. Eluant from the column was directed into the ToF-CIMS as described above. A relative humidity of 20 % was used for this experiment. This humidity condition is similar to that expected for ambient measurements discussed in Sect. 3.2; this condition was chosen to aid interpretation of ambient air data. Humidity effects are discussed in Sect. 3.1.5. Several species co-elute with another compound (m- and p-xylenes; myrcene and camphene; 1-ethyl,3-methylbenzene and 1-ethyl,4-methylbenzene); reported sensitivities and product ions are an average of the two co-eluting species.

Each VOC mixture was sampled twice, once with H_3O^+ and once with NO^+ reagent ion chemistry and instrument settings. Based on the results we evaluated the utility of NO^+ CIMS relative to H_3O^+ CIMS using two metrics. The first metric is sensitivity for individual VOCs. To determine the sensitivity (S), the signals (cps) of all product ions were integrated over the width of the chromatographic peak and sensitivities for the measured VOCs using NO^+ chemistry were calculated relative to the sensitivity using H_3O^+ chemistry ($S_{NO+}/S_{H_3O^+}$). For several VOCs, we also calculated the relative sensitivity when only the most abundant product ion (the quantitation ion) is measured (Table 2b). Because only one concentration was sampled, this metric relies on sensitivity being linear with concentration. Linear sensitivity is a reasonable assumption for the NO^+ and H_3O^+ ToF-CIMS because separate multiple-point calibrations for select VOCs showed a linear response (Sect. 3.1.4, Fig. S10), H_3O^+ CIMS has demonstrated linear sensitivity over a wide range of concentration (de Gouw and Warneke, 2007; Sulzer et al., 2014; Yuan et al., 2016), and the NO^+ CIMS agrees well with an independent technique over a range of atmospheric concentrations (Sect. 3.2.2).

The second metric is the simplicity of spectra. In an ideal instrument, each VOC would produce only one product ion, and each ion mass would be produced by only one VOC. However, using NO^+ and H_3O^+ reagent ions, fragmentation of product ions does occur. As a metric for the complexity of the product ion distribution resulting from particular VOCs, we determined the fraction of the most abundant ion to the total signal from this VOC (F) and discuss (F_{NO^+}) relative to ($F_{H_3O^+}$). Figure S3 contains a comparison of F_{NO^+} and $F_{H_3O^+}$ and an example product ion distribution. A larger value of this ratio means that NO^+ reagent ion chemistry creates a simpler product ion distribution for that particular VOC. This metric does not indicate whether a particular product ion is produced by only one VOC. Uniqueness of product ions is discussed in Sect. 3.1.2. The NO^+ CIMS product ion distributions of 25 atmospherically relevant VOCs are reported in Table 2.

Figure 3 summarizes the comparison between NO^+ and H_3O^+ reagent ion chemistry for the two metrics. On the y axis the spectrum simplicity metric and on the x axis the sensitivity metric are shown.

Branched alkanes and most cyclic alkanes are detected with far greater sensitivity using NO^+ chemical ionization than with H_3O^+ chemical ionization. Aromatics and alkenes are detected slightly more sensitively, and, on average, ketones are detected slightly less sensitively. Alcohols are detected more sensitively, by at least a factor of 2, with the

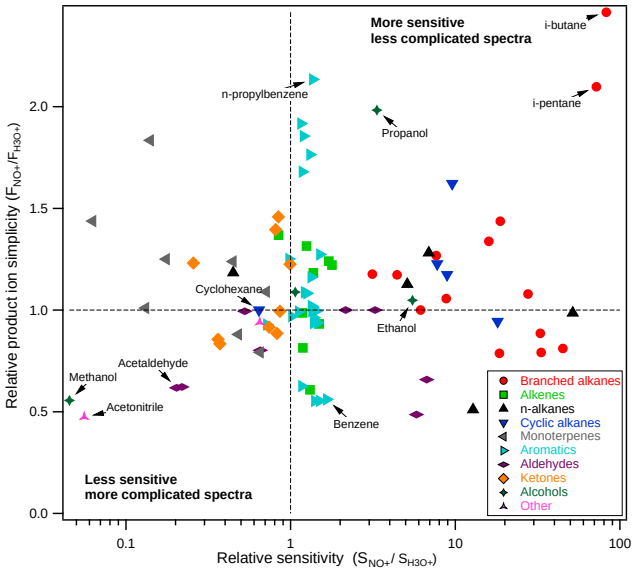

Figure 3. Comparison of production ion distribution and sensitivity of VOCs using NO^+ and H_3O^+ reagent ion chemistry, at a relative humidity of 20 %.

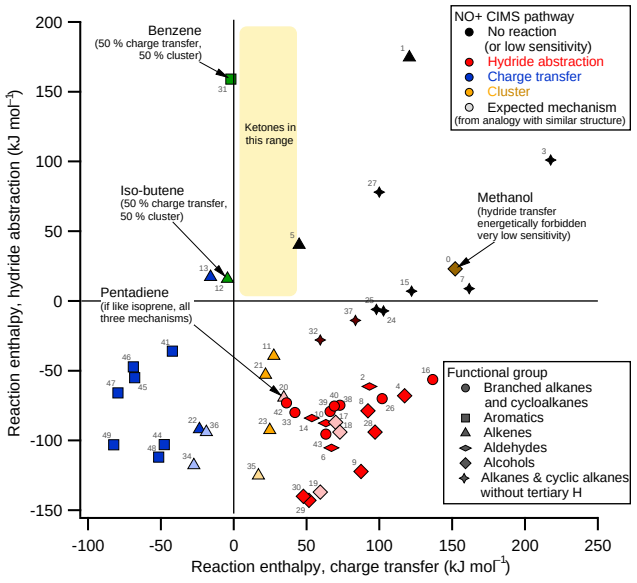

Figure 4. VOC–NO^+ reaction mechanism dependence on charge transfer and hydride transfer reaction enthalpy. VOC identification is indicated by the small numbers and is listed in Table 1. Hydride abstraction enthalpies for ketones are not known but can be assumed to be positive based on structural considerations (lack of tertiary hydrogen). Ion thermodynamic information is available for several species whose reaction mechanism was not experimentally verified in this or previous work; an expected mechanism was determined by analogy with a VOC of similar structure. 17 is 1-butanol, by analogy with 1-propanol; 18 is 2-methylpropanol, by analogy with 1-propanol; 19 is 2-butanol, by analogy with 2-propanol; 20 is 1,4-pentadiene, by analogy with isoprene; 34 is 4-methyl-2-pentene, by analogy with 2-pentene; 35 is 3-methyl-1-pentene, by analogy with 1-hexene; 36 is 2,3,-dimethyl-1-butene, by analogy with isobutene.

exception of methanol. The lower sensitivity to methanol is consistent with slower reaction kinetics reported in the literature (Španěl and Smith, 1997). Monoterpenes and acetonitrile are detected substantially less sensitively.

In comparing the simplicity of the product ion distribution between H_3O^+ and NO^+ chemistry, most branched and cyclic alkanes, ketones, and monoterpenes have a higher fraction of signal on a single product ion (simpler spectra). We also highlight that many alkyl substituted aromatics fragment substantially with H_3O^+ chemistry but do not with NO^+ chemistry. The few exceptions (notably, benzene) create more complicated spectra because an NO^+ cluster product is also present ($m + 30$).

3.1.2 Distribution of product ions

It is somewhat more difficult to predict the ionized VOC products of NO^+ CIMS compared to H_3O^+ CIMS, because NO^+ has three common reaction mechanisms: charge transfer, hydride abstraction, and cluster formation. Groups of VOCs that have similar charge transfer and hydride abstraction enthalpies tend to react with similar ionization mechanisms (Fig. 4). Figure 4 uses thermodynamic information from Lias et al. (1988), as well as mechanistic information from this work (see Table S1 for a list of species) and from SIFT studies (Španěl and Smith, 1996, 1998a, b, 1999; Španěl et al., 1997; Arnold et al., 1998; Francis et al., 2007a, b). Charge transfer occurs when the reaction enthalpy is favorable, regardless of the hydride transfer enthalpy. When the charge transfer enthalpy is close to zero, then NO^+ clustering occurs; when charge transfer is not favorable but hydride transfer is, then hydride transfer will occur. In terms of VOC families, this means that carbonyls participate in two mechanisms: ketones cluster with NO^+, and aldehydes hydride transfer. Branched alkanes exclusively undergo hydride transfer. Aromatics undergo charge transfer and benzene also clusters; alcohols undergo hydride transfer, and alkenes charge transfer, cluster, or hydride transfer depending on the size of the molecule and the location of the double bond within the molecule.

Although Fig. 4 provides a general way to predict the possible mechanisms for a particular VOC, it provides no information about the distribution of the signal between different mechanisms or the degree of fragmentation. The distribution depends strongly on instrumental conditions, which include E/N settings in the ion–molecule reaction region (by far the most important effect), fragmentation and clustering in the ion optics, presence of impurity ions such as O_2^+ from the converted hollow cathode ion source, and relative humidity (Sect. 3.1.5).

In Fig. 5 the product ion distributions of several VOCs determined in this work are compared to three others using NO^+. Studies by the University of Leicester used a much

Table 1. VOC species in Fig. 4 and their charge transfer and hydride transfer reaction enthalpies.

ID no.	Species name	Hydride transfer enthalpy (kJ mol^{-1})	Charge transfer enthalpy (kJ mol^{-1})
0	methanol	22.98	152.05
1	ethene	174.58	120.59
2	acetaldehyde	−61.32	93.20
3	ethane	100.98	217.65
4	ethanol	−68.02	117.31
5	propene	40.17	44.96
6	propanal	−105.32	67.15
7	propane	8.88	161.69
8	n-propanol	−78.72	92.23
9	i-propanol	−122.22	87.41
10	methacrolein	−87.62	63.29
11	1-butene	−39.39	27.59
12	isobutene	15.88	−4.24
13	2-butenes	17.18	−15.82
14	butanal	−84.02	53.64
15	n-butane	6.98	122.14
16	isobutane	−56.32	136.61
17	1-butanol	−87.02	70.04
18	2-methylpropanol	−94.02	72.94
19	2-butanol	−137.02	59.43
20	1,4-pentadiene	−69.32	34.35
21	1-pentene	−53.02	21.80
22	2-pentene	−92.02	−23.54
23	3-methyl-1-butene	−92.52	24.70
24	cyclopentane	−7.22	102.84
25	n-pentane	−6.02	98.02
26	isopentane	−70.02	101.88
27	neo-pentane	77.98	99.95
28	1-pentanol	−94.02	97.05
29	3-methyl-2-butanol	−143.02	51.71
30	3-pentanol	−140.02	47.85
31	benzene	159.08	−1.93
32	cyclohexane	−28.02	59.43
33	methylcyclopentane	−80.02	42.06
34	4-methyl-2-pentene	−117.82	−27.40
35	3-methyl-1-pentene	−125.22	16.98
36	2,3,-dimethyl-1-butene	−94.02	−18.72
37	n-hexane	−13.92	83.55
38	2-methylpentane	−74.72	72.94
39	2,3-dimethylbutane	−79.22	66.18
40	3-methylpentane	−75.42	69.08
41	toluene	−36.02	−42.06
42	methylcyclohexane	−73.02	36.27
43	1,2-dimethyl-cyclopentane	−95.52	63.29
44	ethylbenzene	−103.02	−47.66
45	o-xylene	−55.02	−67.92
46	m-xylene	−47.22	−68.88
47	p-xylene	−65.92	−79.50
48	isopropylbenzene	−111.92	−51.52
49	3-ethyltoluene	−103.12	−82.41
50	acetone		43.03
51	butanone		24.70
52	2-pentanone		11.19
53	3-pentanone		4.44
54	MVK		37.24

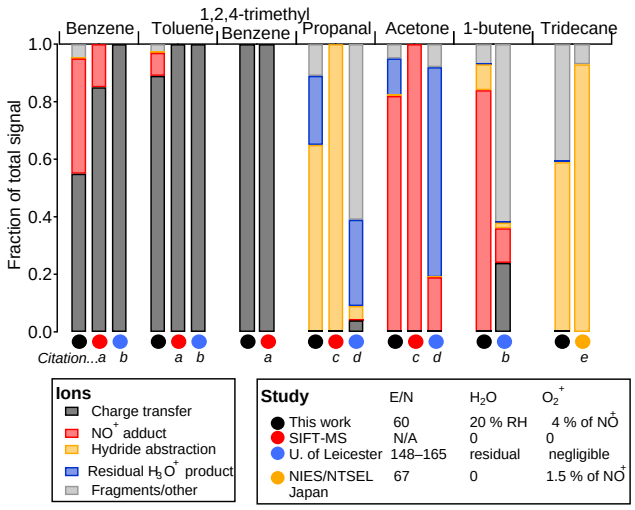

Figure 5. Comparison of product ion distributions between four sets of instrumental and environmental conditions. References: (a) Španěl and Smith (1998b); (b) Blake et al. (2006); (c) Španěl et al. (1997); (d) Wyche et al. (2005); (e) Yamada et al. (2015).

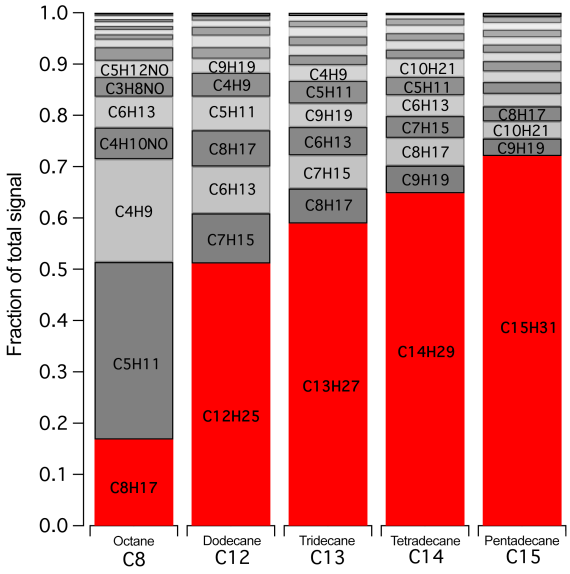

Figure 6. Large (C_{12}–C_{15}) n-alkane product ion distribution, using relative humidity of 20 %. The expected largest mass resulting from hydride abstraction ($m-1$) is highlighted in red. N-octane (C_8) is shown for comparison.

higher E/N ratio in the drift tube, leading to higher fragmentation and lower NO^+ adduct formation compared to this work (Wyche et al., 2005; Blake et al., 2006). Investigation of higher-mass alkanes by Yamada et al. (2015) used similar E/N but achieved lower contaminant O_2^+, which is a likely explanation for the higher degree of fragmentation of tridecane seen in this work. In SIFT-MS studies, without an electric field, fragmentation is minimized and preselection of NO^+ primary ions eliminates contaminant H_3O^+ and O_2^+ and therefore SIFT product ion distributions are generally simpler. These differences highlight the importance of selection of drift tube operating conditions and instrument characterization.

3.1.3 Alkane fragmentation

Small (C_4–C_{10}) branched alkanes cannot be measured by H_3O^+ CIMS. With NO^+ CIMS, these VOCs are detectable but generally fragment to produce several ionic fragments that are common to different species. These masses (for example, m/z 57 $C_4H_9^+$) are produced by many different compounds and are likely not useful for chemically resolved atmospheric measurements. A few masses (e.g., m/z 71 $C_5H_{11}^+$ and m/z 85 $C_6H_{13}^+$) are only produced by a few compounds and were therefore targeted for further investigation in ambient air measurements. Conversely, cyclic alkanes fragment very little. Fig. S4 shows the product ion distributions of several representative aliphatic compounds. We note that the major product ions of cyclic alkanes (M-H) are the same with H_3O^+ and with NO^+ chemistry. However, the mechanism is different: NO^+ ionizes by hydride abstraction, while H_3O^+ ionizes by protonation followed by loss of H_2 (Midey et al., 2003). The H_3O^+ ionization mechanism has a secondary channel consisting of protonation followed by elimination of CH_4 or C_nH_{2n} (Midey et al., 2003). The difference in ionization mechanism is a likely explanation for the lower degree of fragmentation observed using NO^+ chemistry.

Compared to small (C_8 and smaller) alkanes, large (C_{12} and higher) n-alkanes show little fragmentation, with at least 50 % of the total ion signal accounted for by the expected parent mass ($m-1$; Fig. 6). Additionally, the degree of fragmentation decreases with increasing carbon chain length. It is quite difficult to measure these compounds with H_3O^+ CIMS because they fragment extensively and are not detected sensitively (Erickson et al., 2014). NO^+ CIMS could provide a fast, sensitive, chemically specific measurement of these compounds. It should be mentioned that large n-alkanes (C_{10} and larger) are not measurable with the GC interface. Dodecane ($C_{12}H_{26}$), tridecane ($C_{13}H_{28}$), tetradecane ($C_{14}H_{30}$), and pentadecane ($C_{15}H_{32}$) were sampled directly with the NO^+ ToF-CIMS and product ions were identified by correlation with the expected major product ion ($m-1$). The NO^+ ToF-CIMS sensitivity to pentadecane was determined using a permeation source (Veres et al., 2010). Contaminant O_2^+ could potentially reduce the measured parent ion ($[M\text{-}H]^+$) through fragmentation; an alkane measurement corrected for O_2^+ interference would have higher sensitivity and a simpler product ion distribution (e.g., Yamada et al., 2015).

3.1.4 Instrument response factor for select compounds

A calibration factor was determined for various VOCs by (1) direct calibration, (2) estimation from sensitivity relative to H_3O^+ CIMS, or (3) estimation from correlation with GC-

Table 2. Sensitivities and detection limits of NO^+ ToF-CIMS for various VOCs. Additional product ions not used to establish sensitivity are listed in italic. The H_3O^+ ToF-CIMS detection limits in the farthest right column are calculated from separate H_3O^+ ToF-CIMS calibrations as described in Yuan et al. (2016).

(a) Species calibrated directly with NO^+ CIMS; ambient (20 %) relative humidity

	Ion formula (% of total signal)				Back-	Noise	NO^+ sensitivity		NO^+ 1 s	H_3O^+ CIMS 1 s
VOC species	Formula	Mech-anism	(% of total signal)	Exact m/z (Th)	ground cps	scale factor α	ncps/ ppb	cps/ ppb	detection limit	detection limit
Methanol	CH_4ONO^+	$M+NO^+$	(12 %)	62.024	0.70	1.23	0.07	0.67	19 ppb	0.397 ppb
	CH_4OH^+[a]	*$M+H^+$*	*(49 %)*	*33.034*						
	$CH_7O_2^+$[a]	*$M+H_3O^+$*	*(39 %)*	*51.044*						
Acetonitrile	$C_2H_3NNO^+$	$M+NO^+$	(48 %)	71.024	0.49	1.33	3.7	24	540 ppt	45 ppt
	$C_2H_3NH^+$[a]	*$M+H^+$*	*(44 %)*	*42.034*						
	$C_2H_6NO^+$[a]	*$M+H_3O^+$*	*(8 %)*	*60.044*						
Acetaldehyde	$C_2H_3O^+$	$M\text{-}H^-$	(60 %)	43.018	33	1.33	29	146	268 ppt	195 ppt
	$C_2H_5O_2^+$	*$M\text{-}H+H_2O$*	*(13 %)*	*61.028*						
	$C_2H_4OH^+$[a]	*$M+H^+$*	*(11 %)*	*45.034*						
	$C_2H_4ONO^+$	*$M+NO^+$*	*(9 %)*	*74.024*						
Acetone	$C_3H_6ONO^+$	$M+NO^+$	(82 %)	88.039	19	1.16	51	376	73 ppt	97 ppt
	$C_3H_6OH^+$[a]	*$M+H^+$*	*(13 %)*	*59.049*						
Isoprene	$C_5H_8^+$	M^+	(46 %)	68.062	0.76	1.34	44	286	48 ppt	162 ppt
	$C_5H_8NO^+$	*$M+NO^+$*	*(17 %)*	*98.060*						
	$C_5H_7^+$	*$M\text{-}H^-$*	*(7 %)*	*67.054*						
MEK	$C_4H_8ONO^+$	$M+NO^+$	(86 %)	102.055	3.4	1.33	98	767	23 ppt	45 ppt
	$C_4H_8OH^+$[a]	*$M+H^+$*	*(8 %)*	*73.065*						
Benzene[b]	$C_6H_6^+$	M^+	(55 %)	78.046	2.3	1.37	57	391	43 ppt	
	$C_6H_6NO^+$	$M+NO^+$	(40 %)	108.044	2.5	1.72	36	292	74 ppt	96 ppt
	sum				4.8	1.59	93	683	34 ppt	
Toluene	$C_7H_8^+$	M^+	(89 %)	92.062	3.5	1.33	110	825	22 ppt	47 ppt
	$C_7H_8NO^+$	*$M+NO^+$*	*(8 %)*	*122.060*						
o-Xylene	$C_8H_{10}^+$	M^+	(94 %)	106.078	1.3	1.51	121	972	17 ppt	40 ppt
	$C_8H_{10}NO^+$	*$M+NO^+$*	*(5 %)*	*136.076*						
1,2,4-Trimethylbenzene	$C_9H_{12}^+$	M^+	(100 %)	120.093	0.86	1.75	125	1068	17 ppt	45 ppt
n-Pentadecane[c]	$C_{15}H_{31}^+$	$M\text{-}H^-$	(72 %)	211.242	2.7	1.83	48	512	46 ppt	–
	$C_9H_{19}^+$	*fragment*	*(3 %)*	*127.148*						
	$C_{10}H_{21}^+$	*fragment*	*(3 %)*	*141.164*						
	$C_8H_{17}^+$	*fragment*	*(3 %)*	*113.132*						

EIMS (Table 2). Direct calibrations were performed by mixing a known concentration of a VOC from either a permeation cell (pentadecane) or a calibration gas cylinder (other VOCs) into an ambient humidity (∼ 20 %) high-purity air dilution stream. Calibration factors estimated from sensitivity relative to H_3O^+ CIMS were calculated using H_3O^+ ToF-CIMS calibration factors and results from laboratory GC-CIMS experiments (Sect. 3.1.1). Calibration factors for H_3O^+ ToF-CIMS were determined in previous work (Yuan et al., 2016). These calibration factors were multiplied by the relative peak areas determined in Sect. 3.1.1 to obtain estimated NO^+ ToF-CIMS calibration factors. (An example chromatogram and calculation is shown in Fig. S5.) Calibration factors estimated from correlation with GC-EIMS were calculated from the slope of NO^+ ToF-CIMS measurements against GC-EIMS measurements in ambient air (discussed in further detail in Sect. 3.2.2).

In the following discussion we use two metrics of instrument response: cps and normalized cps (ncps). cps is the raw ion count rate of the instrument. Two operations were applied to cps measurements to obtain ncps. First, a duty cycle

Table 2. Continued.

(b) Sensitivity estimated via sensitivity relative to H_3O^+ CIMS; 20 % relative humidity

VOC species	H_3O^+ cps/ ppb	Product ions Formula	Mech-anism	(% of total signal)	Exact m/z (Th)	Relative (NO^+ cps / H_3O^+ cps)	Back-ground cps	Noise scale factor α	NO^+ sensitivity ncps/ ppb	cps/ ppb	NO^+ 1 s detection limit	H_3O^+ CIMS 1 s detection limit
Ethanol	119	$C_2H_5O^+$	$M\text{-}H^-$	(80 %)	45.033	6.2	149	1.37	127	738	105 ppt	1627 ppt
		$C_2H_7O_2^+$	*M-H+H_2O*	*(15 %)*	*63.044*							
Methyl-cyclohexane	27	$C_7H_{13}^+$	$M\text{-}H^-$	(98 %)	97.101	17	6.6	1.32	53	448	50 ppt	943 ppt
		$C_6H_{11}^+$	*fragment*	*(2 %)*	*83.086*							
MVK	539	$C_4H_6ONO^+$	$M+NO^+$	(100 %)	100.039	0.38	4	1.71	24	202	112 ppt	85 ppt
Pentanone	770	$C_5H_{10}ONO^+$	$M+NO^+$	(83 %)	116.071	1.18	4.4	1.32	97	906	21 ppt	47 ppt
		$C_5H_{10}OH^+$[a]	*$M+H^+$*	*(7 %)*	*87.080*							
α-Pinene	262	$C_{10}H_{16}^+$	M^+	(59 %)	136.125	0.28	0.39	1.69	7.3	73	233 ppt	67 ppt
		$C_7H_8^+$	*fragment*	*(24 %)*	*92.062*							
		$C_7H_9^+$	*fragment*	*(11 %)*	*93.070*							
		$C_{10}H_{16}H^+$[a]	*$M+H^+$*	*(7 %)*	*137.132*							

(c) Sensitivity estimated via correlation with GC-EIMS; ambient (20 %) relative humidity

VOC species	Product ions Formula	Mech-anism	(% of total signal)	Exact m/z (Th)	Correlation with GC (R^2)	Back-ground cps	Noise scale factor α	NO^+ Sensitivity ncps/ ppb	cps/ ppb	NO^+ 1 s detection limit
Propanal	$C_3H_5O^+$	$M\text{-}H^-$	(65 %)	57.033	0.928	11	1.40	170	1057	26 ppt
	$C_3H_7O_2^+$[a]	*M-H+H_2O*	*(17 %)*	*75.044*						
	$C_3H_6OH^+$[a]	*$M+H^+$*	*(7 %)*	*59.049*						
Methacrolein + crotonaldehyde	$C_4H_5O^+$	$M\text{-}H^-$	(64 %)	69.033	0.984	4.1	1.37	48	325	60 ppt
	$C_4H_6ONO^+$	*$M+NO^+$*	*(16 %)*	*100.039*						
	$C_3H_5^+$	*fragment*	*(10 %)*	*41.039*						
Isopentane	$C_5H_{11}^+$	$M\text{-}H^-$	(82 %)	71.086	0.888	23	1.36	101	706	49 ppt
	$C_3H_7^+$	*fragment*	*(11 %)*	*43.054*						
Methylcyclo-pentane	$C_6H_{11}^+$	$M\text{-}H^-$	(99 %)	83.086	0.961	7.4	1.34	154	1225	18 ppt
C_5 aldehydes	$C_5H_9O^+$	$M\text{-}H^-$	(49 %)	85.065	0.936	9.8	1.38	119	904	28 ppt
	$C_4H_9^+$	*fragment*	*(22 %)*	*57.070*						
	$C_5H_{11}O_2^+$[a]	*M-H+H_2O*	*(19 %)*	*103.075*						
2- and 3-methylpentane	$C_6H_{13}^+$	$M\text{-}H^-$	(82 %)	85.101	0.978	16	1.34	122	981	30 ppt
	$C_3H_7^+$	*fragment*	*(10 %)*	*43.054*						
	$C_4H+_9^+$	*fragment*	*(4 %)*	*57.070*						
Hexanal	$C_6H_{11}O^+$	$M\text{-}H^-$	(49 %)	99.080	0.945	10	1.47	160	1270	22 ppt
	$C_6H_{13}O_2^+$[a]	*M-H+H_2O*	*(23 %)*	*117.091*						
	$C_5H_{11}^+$	*fragment*	*(15 %)*	*71.086*						
Styrene	$C_8H_8^+$	M^+	(100 %)	104.062	0.949	0.62	1.47	112	966	15 ppt
Benzaldehyde	$C_7H_5O^+$	$M\text{-}H^-$	(100 %)	105.033	0.923	12	1.37	75	621	43 ppt

[a] Product from residual H_3O^+. [b] Both product ions can be unambiguously assigned to benzene. We therefore report also the counting statistics and limit of detection for the sum of the two ions. [c] For technical reasons, pentadecane sensitivity was determined in dry air.

correction was applied (Chernushevich et al., 2001):

$$I_{\text{corr}} = \text{cps} \times \sqrt{\frac{m/z_{\text{reference}}}{m/z}}, \quad (1)$$

where I_{corr} is the duty-cycle-corrected ion count rate and $m/z_{\text{reference}}$ is an arbitrary reference mass (in this work $m/z_{\text{reference}} \equiv 55$). The duty-cycle correction accounts for differences in ion residence time in the extraction region of

the ToF and eliminates a mass-dependent sensitivity bias. Then, measurements were normalized to the duty-cycle-corrected NO^+ (primary ion) measurement, which typically has count rates on the order of 10^6 above that of VOCs:

$$\text{ncps} = 10^6 \frac{I_{\text{corr}}}{\text{NO}^+_{\text{corr}}}. \quad (2)$$

The normalization removes variability due to fluctuations in the ion source and detector. In calculating limits of detection, we use duty-cycle-uncorrected cps, as this best reflects the fundamental counting statistics of the instrument. In reporting ambient air measurements, we use ncps. The ncps measurement reduces several significant instrumental biases and better reflects VOC abundances in air.

Limits of detection at 1 Hz measurement frequency were calculated by finding the mixing ratio at which the signal-to-noise ratio (S/N) is equal to 3. The calculation can be expressed by (Bertram et al., 2011; Yuan et al., 2016)

$$\frac{S}{N} = 3 = \frac{C_{\text{f}}[X]_{\text{lod}}t}{\alpha \times \sqrt{C_{\text{f}}[X]_{\text{lod}}t + 2Bt}}, \quad (3)$$

where C_{f} is the instrument response factor, in cps per ppb; $[X]_{\text{lod}}$ is the limit-of-detection mixing ratio of species X in ppb; t is the sampling period of 1 s; α is the scaling factor of noise compared to expected Poissonian counting statistics; and B is the background count rate in cps. The scaling factor α is generally greater than 1 because high-resolution peak overlap and fitting algorithms create additional noise (Cubison and Jimenez, 2015). For comparison, H_3O^+ ToF-CIMS limits of detection, using the same ToF-CIMS instrument, are included where available.

Aliphatics and aromatics are generally detected quite sensitively. Aromatics have sub-100 ppt detection limits and are detected slightly more sensitively with NO^+ CIMS than with H_3O^+ CIMS, with NO^+ detection limits generally about 30 % lower. Aliphatic species are detected with quite low detection limits (less than 50 ppt) and with substantially better sensitivity than H_3O^+: the detection limit of methylcyclohexane using NO^+ is a factor of 27 lower than with H_3O^+.

Aldehydes and ketones also have detection limits of around 100 ppt or less, with the exception of acetaldehyde (lod = 355 ppt). The higher detection limit of acetaldehyde is due to a somewhat higher instrumental background and a lower response factor that is consistent with reaction kinetics (Španěl et al., 1997). Methanol has a very high detection limit (19 ppb); this is expected from the anomalously low rate constant of the methanol–NO^+ reaction (Španěl and Smith, 1997). In contrast, ethanol is detected far more sensitively with NO^+ than with H_3O^+, with a detection limit of 105 ppt (compared to 1600 ppt for H_3O^+).

3.1.5 Humidity dependence

Humidity-dependent behaviors of primary ions and selected VOCs (acetaldehyde, acetone, isoprene, 2-butanone, benzene, toluene, o-xylene, and 1,3,5-trimethylbenzene) were determined by diluting a VOC calibration standard into humidified air to reach approximately 10 ppb mixing ratio, then sampling directly with the NO^+ ToF-CIMS. Air temperature was 27 °C. Product ion and signal dependencies on humidity for selected primary ions and VOCs are shown in Fig. 7 (additional species are included in Fig. S6). As relative humidity increases, NO^+ (m/z 30) remains relatively constant, while protonated water and protonated water clusters (especially m/z 37, $H_5O_2^+$) increase. As the abundance of H_3O^+ in the drift tube increases, one might expect to see increased products of VOC reaction with H_3O^+ with a corresponding decrease in NO^+ products. Although an increase of H_3O^+ product is seen for some species (e.g., MEK), it is not universally true. For many species, the major effect is that the NO^+ adduct product increases relative to other NO^+ product ions. This effect is especially intense for isoprene, where the isoprene–NO^+ cluster (m/z 98, $C_5H_8NO^+$) increases by a factor of 10 from 0 to 70 % relative humidity. A similar humidity effect, observed during SIFT measurements of alkenes, has been reported previously by Diskin et al. (2002), who attributed the effect to better stabilization of excited intermediary $(NO^+ \cdot R)^*$ ions by H_2O. A full investigation of this effect is beyond the scope of this paper. In lieu of a complete theoretical understanding of humidity effects, we suggest that an experimental humidity correction could be applied as in Yuan et al. (2016).

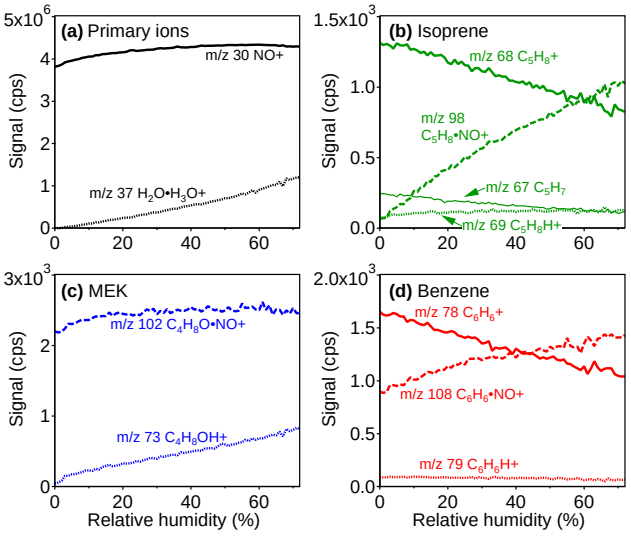

Figure 7. Humidity dependence of primary ions and selected VOCs. **(a)** NO^+ and water clusters; **(b)** isoprene; **(c)** methyl ethyl ketone (MEK); **(d)** benzene.

3.2 Measurements of urban air

3.2.1 GC-NO^+ CIMS measurements

Measurement of ambient air using the GC interface allowed us to determine which compounds in ambient air produce

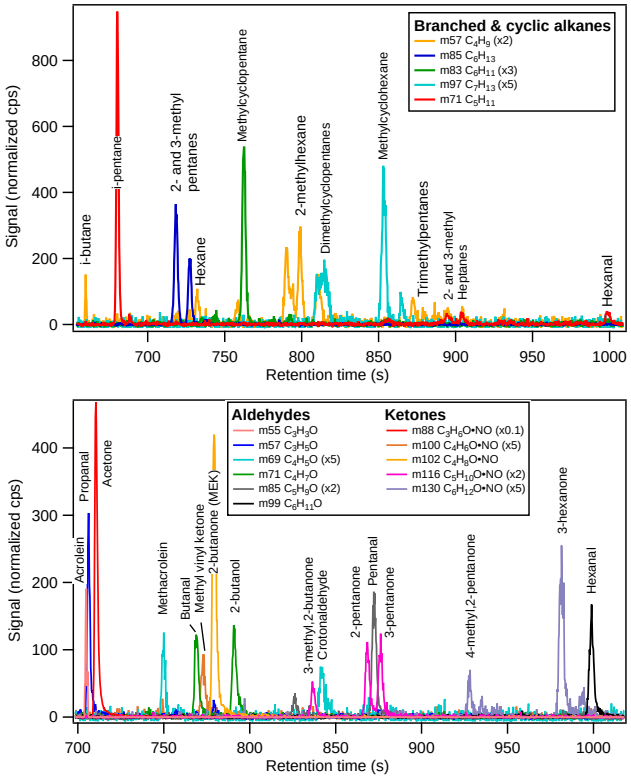

Figure 8. Example GC-CIMS chromatogram of ambient air sample. Masses have been split between two panels for clarity. Top: select masses corresponding to branched and cyclic alkanes. Bottom: select masses corresponding to aldehydes and ketones.

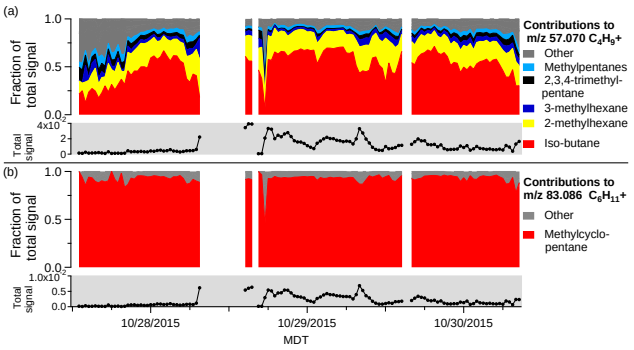

Figure 9. Contributions to two masses based on GC-CIMS measurements of ambient air. "Total signal" is normalized counts per chromatogram. **(a)** m/z 57 $C_4H_9^+$; **(b)** m/z 83 $C_6H_{11}^+$.

which masses. This is the essential link between laboratory measurements of calibration standards and interpretation of ambient NO^+ ToF-CIMS measurements. Ambient air from outside the laboratory was sampled from 27 to 30 October 2015 through an inlet 3 m above ground level and directed through 10 m of 1/2 in. diameter Teflon tubing at a flow rate of 17 standard L min^{-1} (residence time approximately 4 s). The GC interface subsampled this stream. Eluant from the column was directed into the NO^+ ToF-CIMS as described in Sect. 2.1. The laboratory is in an urban area (Boulder, CO) and the inlet was located near a parking lot and loading dock. Absolute instrument background (including the GC interface) was determined by sampling zero air at the beginning and end of the 3-day measurement period. Instrument performance and stability, retention times of selected compounds, and instrument background were checked at least once per day by sampling a 56-component hydrocarbon calibration standard.

Figure 8 shows several masses from a typical chromatogram. In this chromatogram, it is clear, for instance, that the majority of signal from m/z 83 ($C_6H_{11}^+$) can be attributed to one compound (methylcyclopentane). In contrast, m/z 57 ($C_4H_9^+$) is produced from many different compounds with comparable intensities. Aldehydes and ketones appear to be well separated, as expected from the laboratory experiments. Figure 9 summarizes the contributions of different VOCs to several ions (m/z 57, $C_4H_9^+$ and m/z 83 $C_6H_{11}^+$) during the entire 3-day measurement period. M/z 57 ($C_4H_9^+$) has contributions from many different VOCs, and the relative proportions are highly variable. Conversely, m/z 83 ($C_6H_{11}^+$) is mostly attributable to methylcyclopentane during the majority of the 3-day measurement period. M/z 57 ($C_4H_9^+$) does not provide a useful measurement of alkanes, while m/z 83 ($C_6H_{11}^+$) may possibly provide a useful measurement of methylcyclopentane. Corresponding figures for other masses can be found in the supplemental information (Figs. S7–S9). Table 3 summarizes our assessment of key ions.

3.2.2 NO^+ CIMS vs. GC-EIMS measurement comparison

Measurements using the GC interface do not provide any information about the fast time response capability of the NO^+ ToF-CIMS. Additionally, not all compounds detectable by NO^+ CIMS and present in ambient air can be transmitted through the GC interface. Simultaneous GC-EIMS and NO^+ ToF-CIMS measurements were conducted to investigate fast NO^+ measurements, determine whether there are any significant interferences to key NO^+ masses, and explore NO^+ CIMS response to VOCs not transmittable through the GC interface.

Ambient air was sampled into the laboratory as described in the previous section. The GC-EIMS and the NO^+ ToF-CIMS were run as separate instruments and subsampled the 17 SLPM flow at the same point. Measurements were taken from 4 to 6 November 2015. The GC-EIMS instrument was operated on a 30 min schedule. GC-EIMS instrument background was determined from zeros taken at the beginning and end of the 3-day measurement period. The 56-component hydrocarbon calibration standard was sampled once per day. The NO^+ ToF-CIMS measured at 1 Hz frequency. Instru-

Table 3. Assessment of significant product ions investigated by GC-NO^+ CIMS and parallel GC-EIMS and NO^+ CIMS measurement of ambient air. Masses in bold can be unambiguously assigned to a single VOC or a structurally related, correlated group of VOCs.

			Correlation with parallel GC-EIMS	
Ion formula (Th)	Exact mass	Assessment from series GC-NO^+ ToF-CIMS	R^2	Slope (ppbv ppbv^{-1})
$C_3H_5^+$	41 039	Several non-correlated species		
$C_2H_3O^+$	43.018	**Acetaldehyde**	**0.942**	**0.892**
$C_3H_7^+$	43.054	Several non-correlated species		
$C_2H_5O^+$	45.033	**Ethanol**	**0.998**	
$C_4H_6^+$	**54.046**	**Propyne**[1]		
$C_4H_8^+$	56.062	Several non-correlated species		
$C_3H_5O^+$	**57.033**	**Propanal**	**0.928**	
$C_4H_9^+$	57.070	Several non-correlated species		
$C_3H_7O^+$	59.049	Interference from acetone; If accounted for, sum of C_3 alcohols		
$CH_4NO_2^+$	**62.024**	**Methanol, but poor sensitivity**	**0.904**	**1.25**
$C_5H_6^+$	66.046	Interference from benzene; if accounted for, cyclopentadiene		
$C_4H_4O^+$	**68.026**	**Furan**[2]		
$C_5H_8^+$	68.062	Possibly isoprene[3]		
$C_4H_5O^+$	**69.033**	**Methacrolein + crotonaldehyde**[4]	**0.984**	
$C_5H_9^+$	69.070	Several non-correlated species		
$C_5H_{10}^+$	70.078	Possibly the sum of 2-pentenes[3]		
$C_4H_7O^+$	71.049	Several non-correlated species		
$C_5H_{11}^+$	**71.086**	**Isopentane**	**0.888**	
$C_4H_9O^+$	73.065	Several non-correlated species		
$C_6H_6^+$	**78.046**	**Benzene**[5]	**0.987**	**0.847**
$C_5H_6O^+$	82.041	Possibly the sum of 2- and 3-methylfuran[3]		
$C_6H_{11}^+$	**83.086**	**Methylcyclopentane**	**0.961**	
$C_5H_9O^+$	**85.065**	**Sum of C_5 aldehydes**	**0.936**	
$C_6H_{13}^+$	**85.101**	**Sum of 2- and 3-methylpentane**	**0.978**	
$C_4H_8NO^+$	86.060	Several non-correlated species		
$C_5H_{11}O^+$	87.080	C_5 alcohols and ethers; significant interference from minor carbonyl product ions		
$C_3H_6NO_2^+$	**88.039**	**Acetone**	**0.978**	**1.13**
$C_2H_4NO_3^+$	90.019	Possibly acetic acid (chromatography too poor to determine)		
$C_7H_8^+$	**92.062**	**Toluene**	**0.999**	**0.810**
$C_7H_{13}^+$	**97.101**	**Sum of C_7 cyclic alkanes**	**0.917**	
$C_6H_{11}O^+$	**99.080**	**Hexanal**	**0.945**	
$C_7H_{15}^+$	99.117	Possibly the sum of 2- and 3-methylhexane, but poor sensitivity		
$C_4H_6NO_2^+$	**100.039**	**MVK**	**0.950**	
$C_5H_{10}NO^+$	100.076	Possibly the sum of C_5 terminal alkenes, but poor sensitivity		
$C_4H_8NO_2^+$	**102.055**	**MEK**	**0.971**	**0.843**

ment zeros were taken for a 2 min period once every hour (example time series with zeros in Fig. S10). Calibration gas from a 10-component hydrocarbon standard was sampled for 2 min once every 3 h. At the end of the 3-day measurement period, both instruments were disconnected from the ambient air line and sampled air from inside the laboratory for 1.5 h

Table 3. Continued.

Ion formula (Th)	Exact mass	Assessment from series GC-NO^+ ToF-CIMS	Correlation with parallel GC-EIMS	
			R^2	Slope (ppbv ppbv^{-1})
$C_8H_8^+$	**104.062**	**Styrene (vinyl benzene)**	**0.949**	
$C_7H_5O^+$	**105.033**	**Benzaldehyde**	**0.923**	
$C_8H_{10}^+$	**106.078**	**Sum of C_8aromatics**	**0.952**	**0.746**
$C_6H_6NO^+$	**108.044**	**Benzene**[5]		
$C_8H_{15}^+$	111.117	Possibly the sum of C_2 alkyl-substituted cyclohexanes[6]	0.761	
$C_7H_{13}O^+$	**113.096**	**Heptanal**[2]		
$C_8H_{17}^+$	113.132	Possibly the sum of methylheptanes, but poor sensitivity		
$C_5H_{10}NO_2^+$	**116.071**	**Sum of C_5ketones**	**0.945**	
$C_9H_{10}^+$	118.078	Possibly the sum of methylstyrene isomers[3]		
$C_9H_{12}^+$	120.093	Sum of C_9 aromatics; scatter possibly due to disparity in response factors	0.600	
$C_8H_{15}O^+$	**127.112**	**Octanal**[2]		
$C_6H_{12}NO_2^+$	130.086	Possibly the sum of C_6 ketones[3]		
$C_{10}H_{14}^+$	134.109	Possibly the sum of C_{10} aromatics		
$C_{10}H_{16}^+$	136.125	Monoterpenes plus unknown interference; possibly adamantane from vehicle exhaust	0.584	
$C_7H_{14}NO_2^+$	144.102	Heptanone[2]		

[1] Cross-comparison with independent GC-EIMS not possible due to chromatographic quantitation ion overlap with neighboring peaks. [2] Cross-comparison with independent GC-EIMS not possible due to EIMS quadrupole selected-ion scan window restrictions. [3] Concentrations too low in ambient air to determine. [4] Winter urban air sampled was likely influenced by local domestic biomass burning; crotonaldehyde may be a smaller fraction of signal in other environments. [5] Benzene correlation using sum of m108 $C_6H_6NO^+$ and m78 $C_6H_6^+$. [6] With exclusion of single outlier, $R^2 = 0.831$.

(three GC samples) to investigate the NO^+ ToF-CIMS response to air with a VOC composition substantially different from urban air.

For all comparisons between the two instruments, the 1 Hz NO^+ ToF-CIMS measurements were averaged over the 5 min GC-EIMS collection period. The NO^+ ToF-CIMS was calibrated using air with ambient humidity (approximately 20 %) for the 10 species listed in Table 2a, and no further humidity correction was applied. Correlations between independent GC and calibrated CIMS measurements generally show a high correlation coefficient ($R^2 > 0.9$) and slopes close to 1 (examples in Fig. 10a, b). This demonstrates that an adapted NO^+ CIMS instrument retains sensitive measurement of atmospherically important species such as aromatics that are often targeted using PTR-MS and in addition can detect compounds such as isopentane, sum of 2- and 3-methylpentane, methylcyclopentane, and sum of C_7 cyclic alkanes (Fig. 10c–f) that are usually not detected with PTR-MS. Slopes for calibrated VOCs, and correlation coefficients (R^2) for all VOCs investigated, are included in Table 3. The good agreement also indicates that humidity dependence of sensitivity is likely not a severe effect for most species; however, addressing and quantifying this effect should be a priority for future work.

To assess the ability of the NO^+ ToF-CIMS to separate ketones and aldehydes, we explore measurements of propanal and acetone. The separate measurement of these two species is a good test case because the two peaks are chromatographically well resolved on the GC-EIMS, there are few isomers of C_3H_6O (of which acetone and propanal are likely the only atmospherically relevant species), and independent measurements of these two species are interesting for scientific reasons: aldehydes are generally much more reactive with OH than their ketone isomers and may have significantly different behavior in the atmosphere (Atkinson and Arey, 2003).

A time series of propanal and acetone is shown in Fig. 11a. The two compounds have clearly different behavior in the atmosphere: there is fast (seconds to minutes), high variability in the acetone measurement that is not seen in the propanal measurement, and the longer-term ($\sim$hours) variability of acetone and propanal is not the same. The fast, high spikes in acetone may come from local sources such as exhaust from chemistry labs in the building. The acetone comparison between the GC-EIMS and the NO^+ ToF-CIMS has a slope of 1.13, a correlation coefficient R^2 of 0.978, and negligible

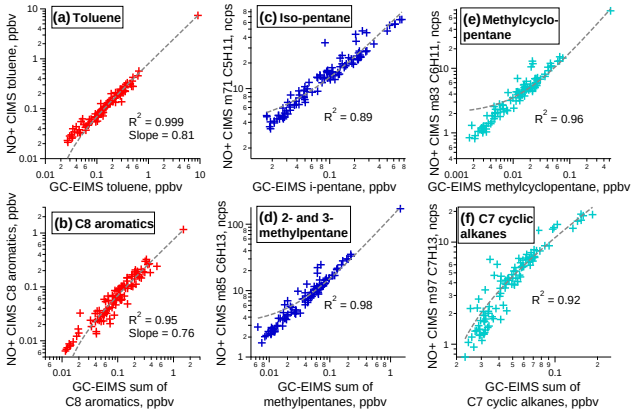

Figure 10. Correlations between VOCs measured with GC-EIMS and NO^+ ToF-CIMS in ambient air. The 1 Hz NO^+ ToF-CIMS measurement is averaged to the 5 min GC collection period. Orthogonal least-squares linear best fits (ODR best fit) are shown with dashed lines. The lines appear curved due to log-scale axes. For several compounds (e.g., methylcyclopentane, 2- and 3-methylpentane), the single high outlier pulls the best fit slightly away from the data points at low mixing ratios. **(a)** Toluene. **(b)** C_8 aromatics: sum of ethylbenzene, o-xylene, m-xylene, and p-xylene. **(c)** Isopentane. **(d)** Sum of 2-methylpentane and 3-methylpentane. **(e)** Methylcyclopentane. **(f)** C_7 cyclic alkanes: sum of methylcyclohexane, ethylcyclopentane, and dimethylcyclopentane.

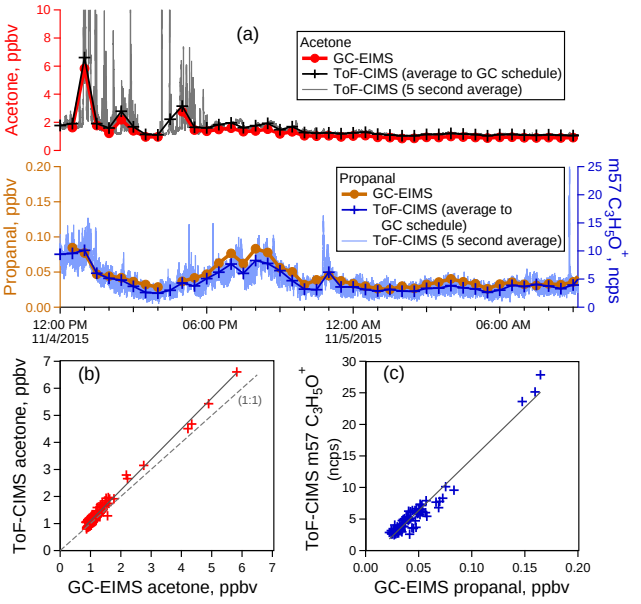

Figure 11. (a) Time series of acetone and propanal measurements from NO^+ ToF-CIMS and GC-EIMS in ambient air. Measurements shown include the GC-EIMS measurement (5 min sample every 30 min, circle markers), the NO^+ ToF-CIMS measurement averaged over the 5 min GC sampling period (cross markers), and the NO^+ ToF-CIMS measurement averaged to a 5 s running mean. **(b)** Correlation between NO^+ ToF-CIMS and GC-EIMS measurement of acetone. **(c)** Correlation between NO^+ ToF-CIMS and GC-EIMS measurement of propanal.

offset. The comparison between the GC and CIMS propanal measurements has an R^2 of 0.928 (Fig. 11b, c).

Several episodes occurred with elevated high-mass n-alkane masses (m/z 169 $C_{12}H_{25}^+$, dodecane; m/z 183 $C_{13}H_{27}^+$, tridecane; m/z 197 $C_{14}H_{29}^+$, tetradecane; m/z 211 $C_{15}H_{31}^+$, pentadecane). Two examples are shown in Fig. 12. The episodes show high temporal and compositional variability. The inlet was downwind from a parking lot and next to a loading dock and electric power generator for the building, and it is likely that the elevated C_{12}–C_{15} alkanes are from any or all of these sources. An ambient air measurement of these species is particularly interesting because they have been implicated in efficient secondary organic aerosol production from diesel fuel exhaust (Gentner et al., 2012).

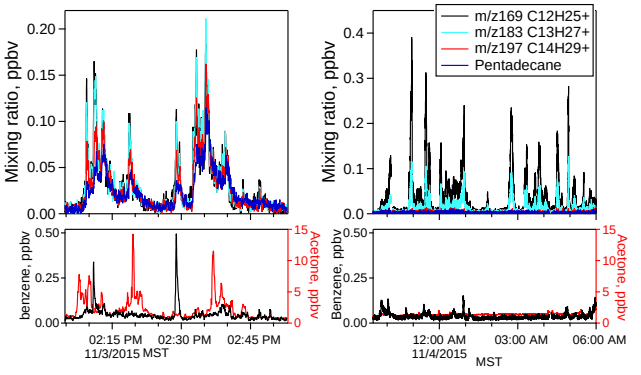

Figure 12. Episodes with elevated high-mass alkane masses in ambient air. Mixing ratios for m/z 169 $C_{12}H_{25}^+$ (dodecane), m/z 183 $C_{13}H_{27}^+$ (tridecane), and m/z 197 $C_{14}H_{29}^+$ (tetradecane) are shown in approximate ppbv, assuming the same instrument calibration factor as pentadecane. Additional VOC species (benzene, acetone) are shown in the bottom panels for context.

4 Summary and conclusions

In summary, an H_3O^+ ToF-CIMS (PTR-MS) instrument was easily and inexpensively converted into an NO^+ CIMS by replacing the reagent source gas and modifying the ion source and drift tube voltages. The usefulness of NO^+ CIMS for atmospheric VOC measurement was then evaluated by (1) using a GC interface to determine product ion distributions for nearly 100 VOCs and compare the sensitivity and simplicity of spectra to H_3O^+ CIMS; (2) measuring ambient air with a GC interface, to map product ions to their VOC precursors and determine which ions may be useful for chemically specific measurement; and (3) measuring ambient air directly, to evaluate chemical specificity and investigate fast (1 Hz) time measurement of new compounds. Additionally, the NO^+ CIMS response to C_{12}–C_{15} n-alkanes and to vari-

able humidity was determined in some detail. Further work is needed to better understand the humidity dependence.

NO^+ CIMS is a valuable technique for atmospheric measurement because it can separate small carbonyl isomers, it can provide fast and chemically specific measurement of cyclic and a few important branched alkanes (notably, isopentane and methylpentane) that cannot be detected by PTR-MS, it can measure alkyl-substituted aromatics with less fragmentation than H_3O^+ CIMS, and it can detect larger (C_{12}–C_{15}) alkanes. With NO^+ CIMS significant fragmentation of most small alkanes does occur, making them difficult to measure quantitatively. There are also interferences on many alcohols (with the exception of ethanol) and butanal. Additionally, it is worth considering that $VOC \cdot NO^+$ cluster formation moves certain species into a higher mass range. This may be a drawback because the number of possible isobaric compounds increases with mass, and it may be more difficult for high-resolution peak-fitting algorithms to separate species of interest from isobaric interferences (example in Fig. S11). Finally, because there are three different ionization mechanisms (hydride transfer, charge transfer, and NO^+ adduct formation), it may be difficult to determine which VOC precursors correspond to particular ions. NO^+ CIMS may be an extremely useful supplementary approach for specific applications such as studying secondary organic aerosol precursors in vehicle exhaust, investigating emissions from oil and natural gas extraction, identifying additional species in complex emissions such as biomass burning, measuring emissions of oxygenated consumer products and solvents in urban areas, and investigating photochemistry of biogenic VOCs.

The Supplement related to this article is available online at doi:10.5194/amt-9-2909-2016-supplement.

Author contributions. P. Veres and C. Warneke obtained CIRES IRP project funding. B. Yuan, A. Koss, C. Warneke, and J. de Gouw developed the ToF-CIMS instrument. A. Koss converted the instrument from H_3O^+ to NO^+, designed the experiments, collected data, and wrote the manuscript. A. Koss and M. Coggon analyzed data. C. Warneke and J. de Gouw provided guidance on experimental design and interpretation. All authors edited the manuscript.

Acknowledgements. This work was funded by the CIRES Innovative Research Program. A. R. Koss acknowledges additional support from the NSF Graduate Fellowship Program. We would like to thank J. B. Gilman and B. M. Lerner for help with GC operation and data analysis.

Edited by: P. Herckes
Reviewed by: three anonymous referees

References

Agarwal, B., González-Méndez, R., Lanza, M., Sulzer, P., Märk, T. D., Thomas, N., and Mayhew, C. A.: Sensitivity and Selectivity of Switchable Reagent Ion Soft Chemical Ionization Mass Spectrometry for the Detection of Picric Acid, J. Phys. Chem. A, 118, 8229–8236, doi:10.1021/jp5010192, 2014.

Arnold, S. T., Viggiano, A. A., and Morris, R. A.: Rate Constants and Product Branching Fractions for the Reactions of H_3O^+ and NO^+ with C_2-C_{12} Alkanes, J. Phys. Chem. A, 102, 8881–8887, doi:10.1021/jp9815457, 1998.

Atkinson, R. and Arey, J.: Atmospheric degradation of volatile organic compounds, Chem. Rev., 103, 4605–4638, 2003.

Bertram, T. H., Kimmel, J. R., Crisp, T. A., Ryder, O. S., Yatavelli, R. L. N., Thornton, J. A., Cubison, M. J., Gonin, M., and Worsnop, D. R.: A field-deployable, chemical ionization time-of-flight mass spectrometer, Atmos. Meas. Tech., 4, 1471–1479, doi:10.5194/amt-4-1471-2011, 2011.

Blake, R. S., Wyche, K. P., Ellis, A. M., and Monks, P. S.: Chemical ionization reaction time-of-flight mass spectrometry: Multi-reagent analysis for determination of trace gas composition, Int. J. Mass Spectrom., 254, 85–93, doi:10.1016/j.ijms.2006.05.021, 2006.

Buhr, K., van Ruth, S., and Delahunty, C.: Analysis of volatile flavour compounds by Proton Transfer Reaction-Mass Spectrometry: fragmentation patterns and discrimination between isobaric and isomeric compounds, Int. J. Mass Spectrom., 221, 1–7, doi:10.1016/S1387-3806(02)00896-5, 2002.

Chernushevich, I. V., Loboda, A. V., and Thomson, B. A.: An introduction to quadrupole–time-of-flight mass spectrometry, J. Mass Spectrom., 36, 849–865, doi:10.1002/jms.207, 2001.

Cubison, M. J. and Jimenez, J. L.: Statistical precision of the intensities retrieved from constrained fitting of overlapping peaks in high-resolution mass spectra, Atmos. Meas. Tech., 8, 2333–2345, doi:10.5194/amt-8-2333-2015, 2015.

de Gouw, J. and Warneke, C.: Measurements of volatile organic compounds in the earth's atmosphere using proton-transfer-reaction mass spectrometry, Mass. Spectrom. Rev., 26, 223–257, doi:10.1002/mas.20119, 2007.

DeCarlo, P. F., Kimmel, J. R., Trimborn, A., Northway, M. J., Jayne, J. T., Aiken, A. C., Gonin, M., Fuhrer, K., Horvath, T., Docherty, K. S., Worsnop, D. R., and Jimenez, J. L.: Field-Deployable, High-Resolution, Time-of-Flight Aerosol Mass Spectrometer, Anal. Chem., 78, 8281–8289, doi:10.1021/ac061249n, 2006.

Diskin, A. M., Wang, T., Smith, D., and Španěl, P.: A selected ion flow tube (SIFT), study of the reactions of H_3O^+, NO^+ and O_2^+ ions with a series of alkenes; in support of SIFT-MS, Int. J. Mass Spectrom., 218, 87–101, doi:10.1016/S1387-3806(02)00662-0, 2002.

Erickson, M. H., Gueneron, M., and Jobson, B. T.: Measuring long chain alkanes in diesel engine exhaust by thermal desorption PTR-MS, Atmos. Meas. Tech., 7, 225–239, doi:10.5194/amt-7-225-2014, 2014.

Fehsenfeld, F. C., Mosesman, M., and Ferguson, E. E.: Ion–Molecule Reactions in NO^+–H_2O System, J. Chem. Phys., 55, 2120–2125, doi:10.1063/1.1676383, 1971.

Francis, G. J., Milligan, D. B., and McEwan, M. J.: Gas-Phase Reactions and Rearrangements of Alkyl Esters with H_3O^+, NO^+, and $O_2^{\cdot+}$: A Selected Ion Flow Tube Study, J. Phys. Chem. A, 111, 9670–9679, doi:10.1021/jp0731304, 2007a.

Francis, G. J., Wilson, P. F., Milligan, D. B., Langford, V. S., and McEwan, M. J.: GeoVOC: A SIFT-MS method for the analysis of small linear hydrocarbons of relevance to oil exploration, Int. J. Mass Spectrom., 268, 38–46, doi:10.1016/j.ijms.2007.08.005, 2007b.

Gentner, D. R., Isaacman, G., Worton, D. R., Chan, A. W. H., Dallmann, T. R., Davis, L., Liu, S., Day, D. A., Russell, L. M., Wilson, K. R., Weber, R., Guha, A., Harley, R. A., and Goldstein, A. H.: Elucidating secondary organic aerosol from diesel and gasoline vehicles through detailed characterization of organic carbon emissions, P. Natl. Acad. Sci. USA, 109, 18318–18323, doi:10.1073/pnas.1212272109, 2012.

Gilman, J. B., Burkhart, J. F., Lerner, B. M., Williams, E. J., Kuster, W. C., Goldan, P. D., Murphy, P. C., Warneke, C., Fowler, C., Montzka, S. A., Miller, B. R., Miller, L., Oltmans, S. J., Ryerson, T. B., Cooper, O. R., Stohl, A., and de Gouw, J. A.: Ozone variability and halogen oxidation within the Arctic and sub-Arctic springtime boundary layer, Atmos. Chem. Phys., 10, 10223–10236, doi:10.5194/acp-10-10223-2010, 2010.

Gilman, J. B., Lerner, B. M., Kuster, W. C., and de Gouw, J. A.: Source signature of volatile organic compounds from oil and natural gas operations in northeastern Colorado, Environ. Sci. Technol., 47, 1297–1305, doi:10.1021/es304119a, 2013.

Glasius, M. and Goldstein, A. H.: Recent Discoveries and Future Challenges in Atmospheric Organic Chemistry, Environ. Sci. Technol., 50, 2754–2764, doi:10.1021/acs.est.5b05105, 2016.

Goldan, P. D., Kuster, W. C., Williams, E., Murphy, P. C., Fehsenfeld, F. C., and Meagher, J.: Nonmethane hydrocarbon and oxy hydrocarbon measurements during the 2002 New England Air Quality Study, J. Geophys. Res.-Atmos., 109, 2156–2202, doi:10.1029/2003JD004455, 2004.

Graus, M., Müller, M., and Hansel, A.: High Resolution PTR-TOF: Quantification and Formula Confirmation of VOC in Real Time, J. Am. Soc. Mass Spectr., 21, 1037–1044, doi:10.1016/j.jasms.2010.02.006, 2010.

Gueneron, M., Erickson, M. H., VanderSchelden, G. S., and Jobson, B. T.: PTR-MS fragmentation patterns of gasoline hydrocarbons, Int. J. Mass Spectrom., 379, 97–109, doi:10.1016/j.ijms.2015.01.001, 2015.

Inomata, S., Tanimoto, H., and Yamada, H.: Mass Spectrometric Detection of Alkanes Using NO^+ Chemical Ionization in Proton-transfer-reaction Plus Switchable Reagent Ion Mass Spectrometry, Chem. Lett., 43, 538–540, doi:10.1246/cl.131105, 2013.

Jobson, B. T., Alexander, M. L., Maupin, G. D., and Muntean, G. G.: On-line analysis of organic compounds in diesel exhaust using a proton transfer reaction mass spectrometer (PTR-MS), Int. J. Mass Spectrom., 245, 78–89, doi:10.1016/j.ijms.2005.05.009, 2005.

Jordan, A., Haidacher, S., Hanel, G., Hartungen, E., Herbig, J., Märk, L., Schottkowsky, R., Seehauser, H., Sulzer, P., and Märk, T. D.: An online ultra-high sensitivity Proton-transfer-reaction mass-spectrometer combined with switchable reagent ion capability (PTR + SRI − MS), Int. J. Mass Spectrom., 286, 32–38, doi:10.1016/j.ijms.2009.06.006, 2009a.

Jordan, A., Haidacher, S., Hanel, G., Hartungen, E., Märk, L., Seehauser, H., Schottkowsky, R., Sulzer, P., and Märk, T. D.: A high resolution and high sensitivity proton-transfer-reaction time-of-flight mass spectrometer (PTR-TOF-MS), Int. J. Mass Spectrom., 286, 122–128, doi:10.1016/j.ijms.2009.07.005, 2009b.

Karl, T., Hansel, A., Cappellin, L., Kaser, L., Herdlinger-Blatt, I., and Jud, W.: Selective measurements of isoprene and 2-methyl-3-buten-2-ol based on NO^+ ionization mass spectrometry, Atmos. Chem. Phys., 12, 11877–11884, doi:10.5194/acp-12-11877-2012, 2012.

Katzenstein, A. S., Doezema, L. A., Simpson, I. J., Blake, D. R., and Rowland, F. S.: Extensive regional atmospheric hydrocarbon pollution in the southwestern United States, P. Natl. Acad. Sci. USA, 100, 11975–11979, doi:10.1073/pnas.1635258100, 2003.

Keesee, R. G. and Castleman, A. W.: Thermochemical Data on Gas-Phase Ion-Molecule Association and Clustering Reactions, J. Phys. Chem. Ref. Data, 15, 1011, doi:10.1063/1.555757, 1986.

Knighton, W. B., Fortner, E. C., Herndon, S. C., Wood, E. C., and Miake-Lye, R. C.: Adaptation of a proton transfer reaction mass spectrometer instrument to employ NO^+ as reagent ion for the detection of 1,3-butadiene in the ambient atmosphere, Rapid Commun. Mass Sp., 23, 3301–3308, doi:10.1002/rcm.4249, 2009.

Lias, S. G., Bartmess, J. E., Liebman, J. F., Holmes, J. L., Levin, R. D., and Mallard, W. G.: Gas-Phase Ion and Neutral Thermochemistry, J. Phys. Chem. Ref. Data, 17, ISBN: 0-88318-562-8, 1988.

Liu, Y. J., Herdlinger-Blatt, I., McKinney, K. A., and Martin, S. T.: Production of methyl vinyl ketone and methacrolein via the hydroperoxyl pathway of isoprene oxidation, Atmos. Chem. Phys., 13, 5715–5730, doi:10.5194/acp-13-5715-2013, 2013.

Midey, A. J., Williams, S., Miller, T. M., and Viggiano, A. A.: Reactions of O_2^+, NO^+ and H_3O^+ with methylcyclohexane (C_7H_{14}) and cyclooctane (C_8H_{16}) from 298 to 700 K, Int. J. Mass Spectrom., 222, 413–430, doi:10.1016/S1387-3806(02)00996-X, 2003.

Prince, B. J., Milligan, D. B., and McEwan, M. J.: Application of selected ion flow tube mass spectrometry to real-time atmospheric monitoring, Rapid Commun. Mass Sp., 24, 1763–1769, doi:10.1002/rcm.4574, 2010.

Smith, D. and Španěl, P.: Selected ion flow tube mass spectrometry (SIFT-MS) for on-line trace gas analysis, Mass Spectrom. Rev., 24, 661–700, doi:10.1002/mas.20033, 2005.

Španěl, P. and Smith, D.: A selected ion flow tube study of the reactions of NO^+ and O_2^+ ions with some organic molecules: The potential for trace gas analysis of air, J. Chem. Phys., 104, 1893–1899, doi:10.1063/1.470945, 1996.

Španěl, P. and Smith, D.: SIFT studies of the reactions of H3O+, NO^+ and O_2^+ with a series of alcohols, Int. J. Mass Spectrom., 167–168, 375–388, doi:10.1016/S0168-1176(97)00085-2, 1997.

Španěl, P. and Smith, D.: Selected ion flow tube studies of the reactions of H_3O^+, NO^+, and O_2^+ with several amines and some other nitrogen-containing molecules, Int. J. Mass Spectrom., 176, 203–211, doi:10.1016/S1387-3806(98)14031-9, 1998a.

Španěl, P. and Smith, D.: Selected ion flow tube studies of the reactions of H_3O^+, NO^+, and O_2^+ with several aromatic and aliphatic hydrocarbons, Int. J. Mass Spectrom., 181, 1–10, doi:10.1016/S1387-3806(98)14114-3, 1998b.

Španěl, P. and Smith, D.: Selected ion flow tube studies of the reactions of H_3O^+, NO^+, and O_2^+ with several aromatic and aliphatic monosubstituted halocarbons, Int. J. Mass Spectrom., 189, 213–223, doi:10.1016/S1387-3806(99)00103-7, 1999.

Španěl, P., Ji, Y., and Smith, D.: SIFT studies of the reactions of H_3O^+, NO^+ and O_2^+ with a series of aldehydes and ketones,

Int. J. Mass Spectrom., 165–166, 25–37, doi:10.1016/S0168-1176(97)00166-3, 1997.

Sulzer, P., Hartungen, E., Hanel, G., Feil, S., Winkler, K., Mutschlechner, P., Haidacher, S., Schottkowsky, R., Gunsch, D., Seehauser, H., Striednig, M., Jürschik, S., Breiev, K., Lanza, M., Herbig, J., Märk, L., Märk, T. D., and Jordan, A.: A Proton Transfer Reaction-Quadrupole interface Time-Of-Flight Mass Spectrometer (PTR-QiTOF): High speed due to extreme sensitivity, Int. J. Mass Spectrom., 368, 1–5, doi:10.1016/j.ijms.2014.05.004, 2014.

Veres, P., Gilman, J. B., Roberts, J. M., Kuster, W. C., Warneke, C., Burling, I. R., and de Gouw, J.: Development and validation of a portable gas phase standard generation and calibration system for volatile organic compounds, Atmos. Meas. Tech., 3, 683–691, doi:10.5194/amt-3-683-2010, 2010.

Warneke, C., de Gouw, J. A., Lovejoy, E. R., Murphy, P. C., Kuster, W. C., and Fall, R.: Development of Proton-Transfer Ion Trap-Mass Spectrometry: On-line Detection and Identification of Volatile Organic Compounds in Air, J. Am. Soc. Mass Spectrom., 16, 1316–1324, doi:10.1016/j.jasms.2005.03.025, 2005.

Wyche, K. P., Blake, R. S., Willis, K. A., Monks, P. S., and Ellis, A. M.: Differentiation of isobaric compounds using chemical ionization reaction mass spectrometry, Rapid Commun. Mass Spectrom., 19, 3356–3362, doi:10.1002/rcm.2202, 2005.

Yamada, H., Inomata, S., and Tanimoto, H.: Evaporative emissions in three-day diurnal breathing loss tests on passenger cars for the Japanese market, Atmos. Environ., 107, 166–173, doi:10.1016/j.atmosenv.2015.02.032, 2015.

Yuan, B., Koss, A., Warneke, C., Gilman, J. B., Lerner, B. M., Stark, H., and de Gouw, J. A.: A high-resolution time-of-flight chemical ionization mass spectrometer utilizing hydronium ions (H_3O^+ ToF-CIMS) for measurements of volatile organic compounds in the atmosphere, Atmos. Meas. Tech., 9, 2735–2752, doi:10.5194/amt-9-2735-2016, 2016.

Supplement of Atmos. Meas. Tech., 9, 2909–2925, 2016
http://www.atmos-meas-tech.net/9/2909/2016/
doi:10.5194/amt-9-2909-2016-supplement

Atmospheric Measurement Techniques
Open Access
EGU

Supplement of

Evaluation of NO^+ reagent ion chemistry for online measurements of atmospheric volatile organic compounds

Abigail R. Koss et al.

Correspondence to: Abigail R. Koss (abigail.koss@noaa.gov)

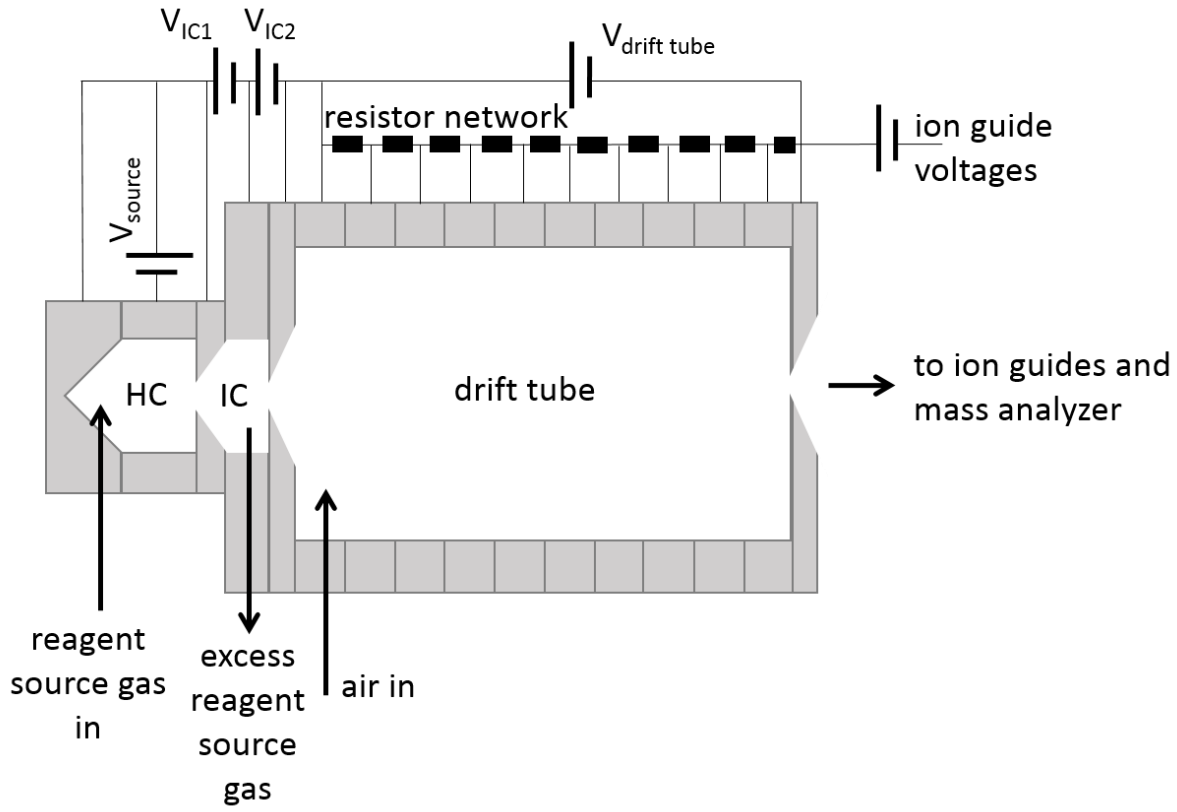

Figure S1. Ion source and drift tube schematic.

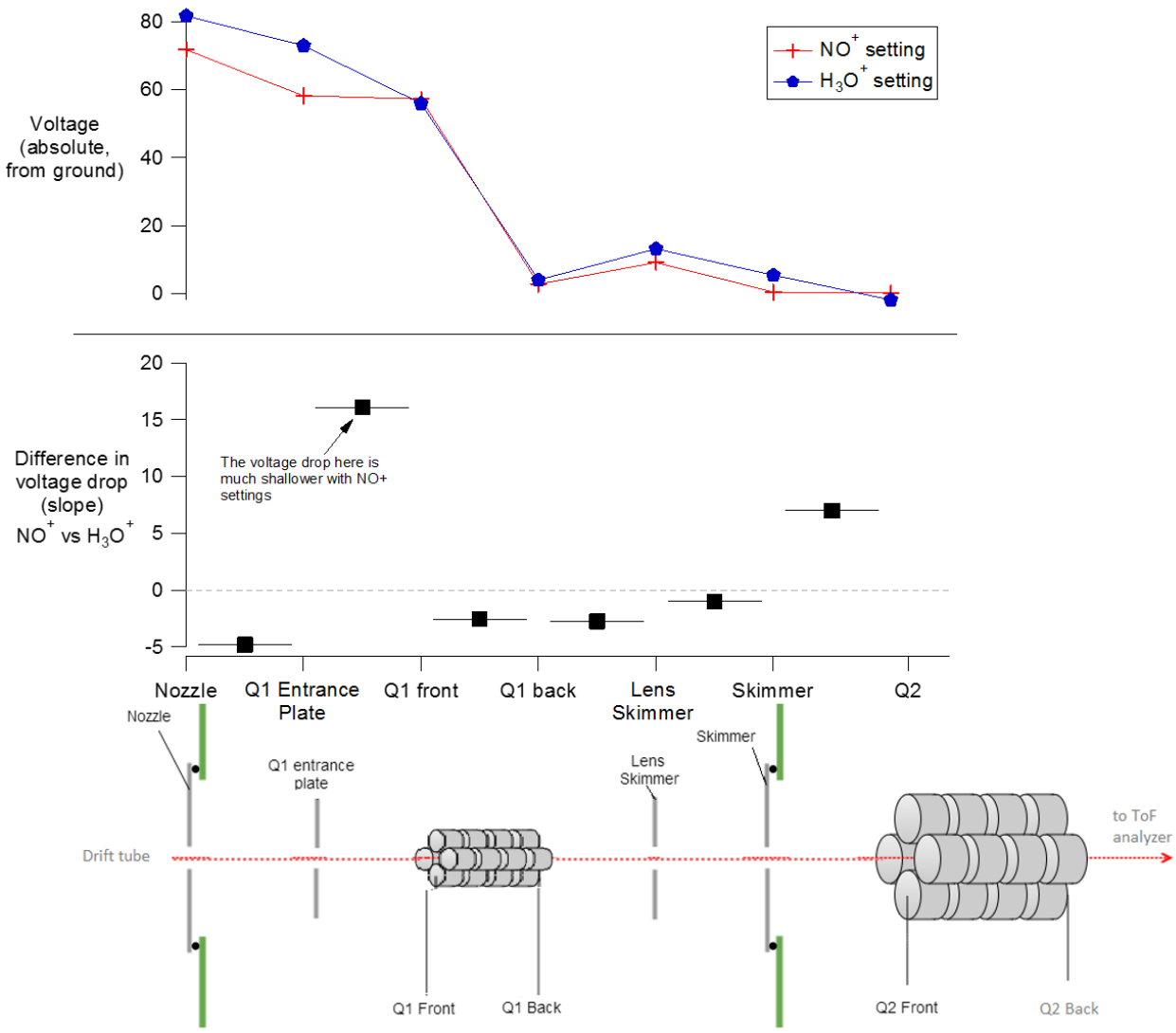

Figure S2. Ion guide voltage settings. The top panel shows the absolute voltage setting (from ground); the middle panel highlights the changes in voltage potential between H_3O^+ and NO^+ settings, and the bottom panel is a cartoon of the ion guide section taken from the CI-API manual (Aerodyne Inc./Tofwerk AG). The horizontal (axial) distances are not to scale.

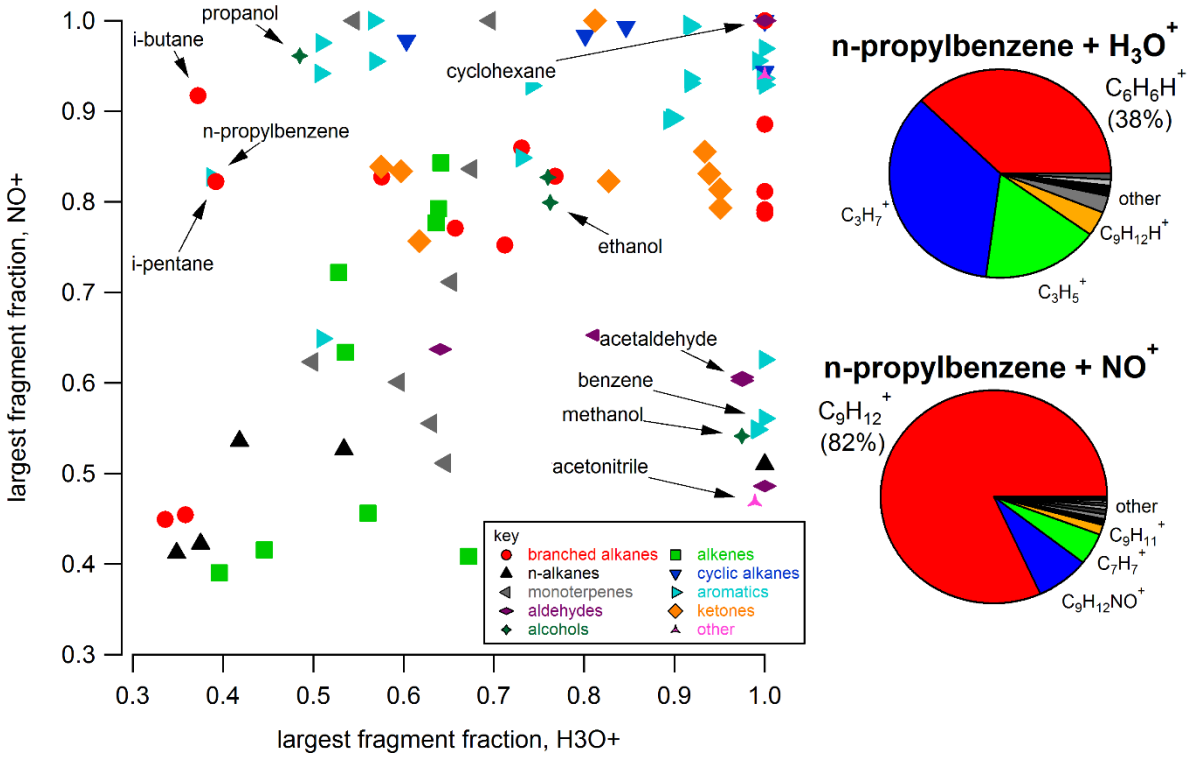

Figure S3. Comparison of product ion distributions between NO^+ CIMS and H_3O^+ CIMS. The complete product ion distribution of n-propylbenzene is shown as an example of a compound with a complex mass spectrum resulting from H_3O^+ chemistry, and a simple mass spectrum resulting from NO^+ chemistry.

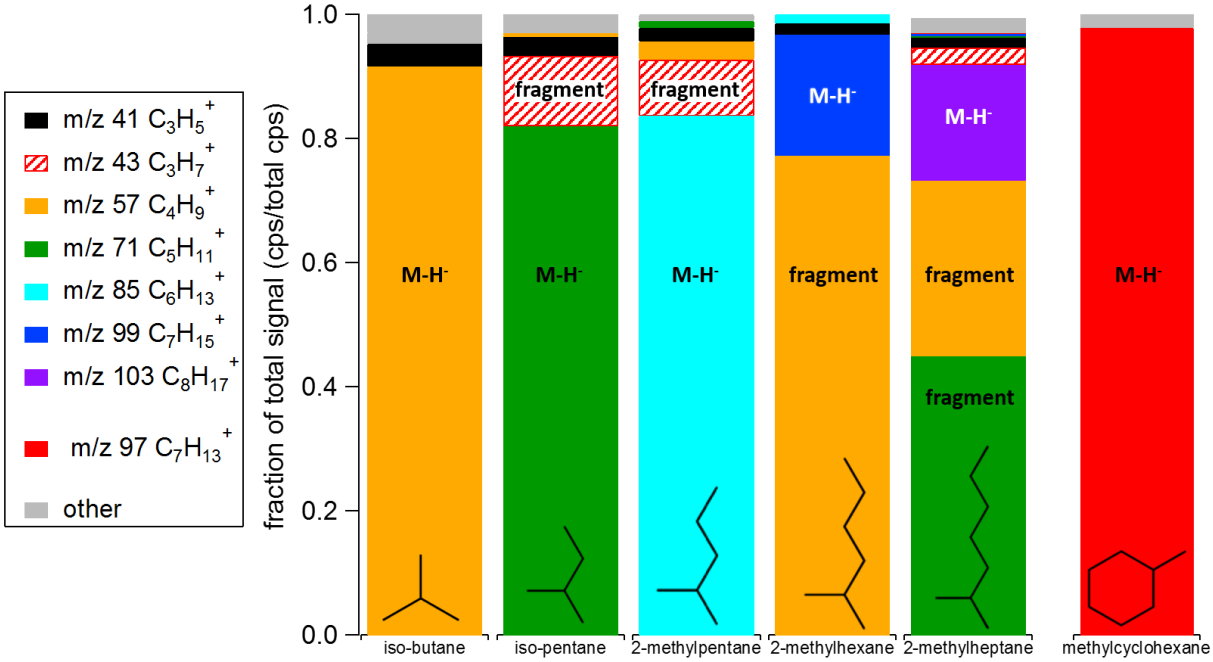

Figure S4. Product ion distributions of selected aliphatic hydrocarbons, at a relative humidity of 20%.

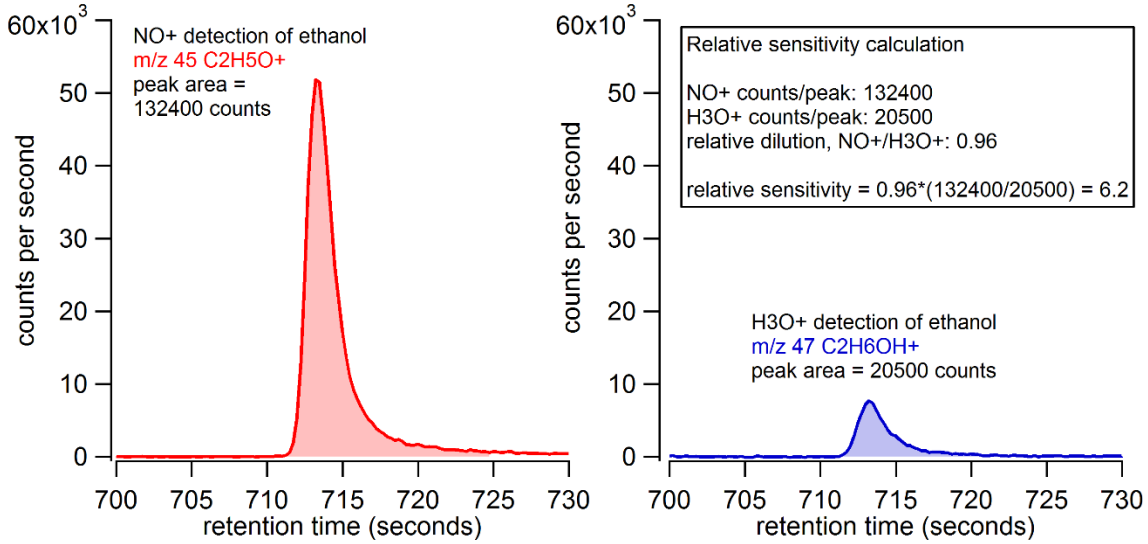

Figure S5. Example chromatograms and relative sensitivity calculation of ethanol for Table 2.

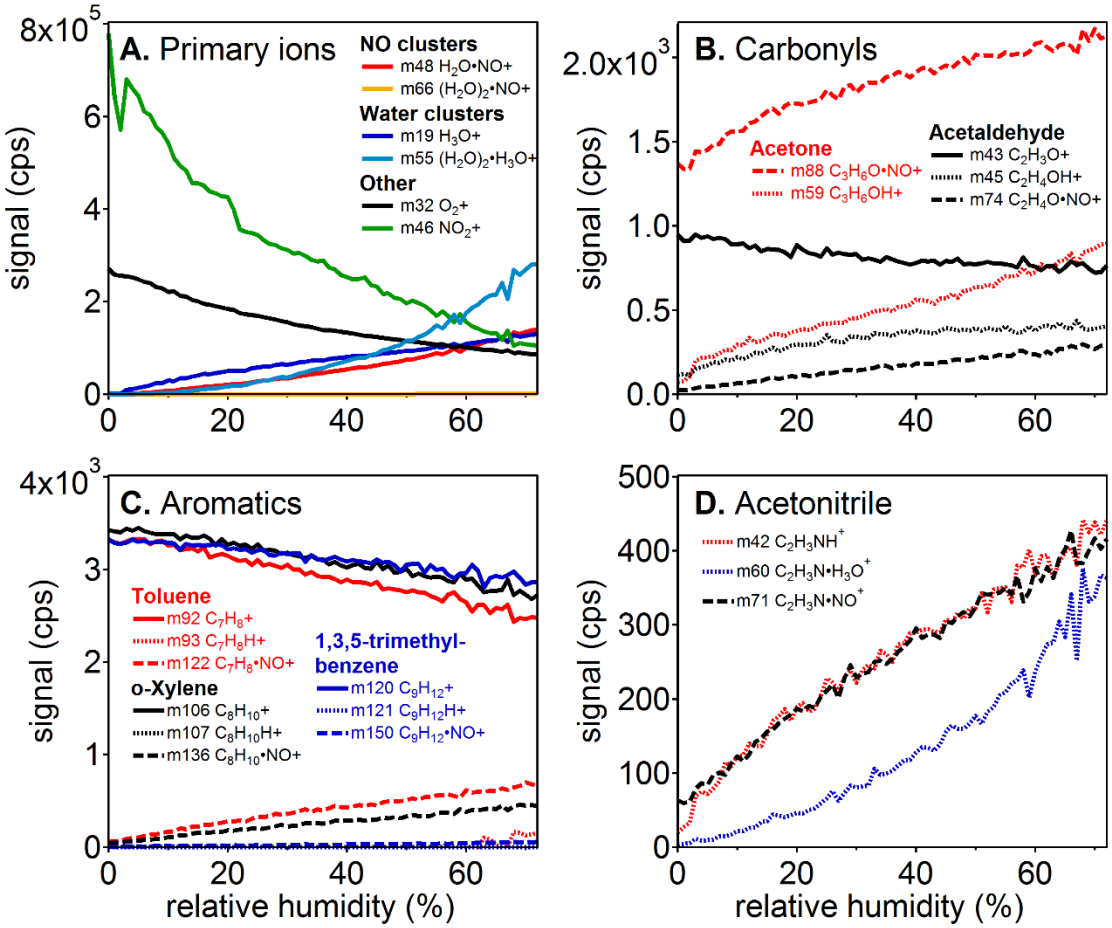

Figure S6. Humidity dependence of primary ions and VOCs. (a) Impurity ions and water clusters. (b) Carbonyls. (c) Aromatics. (d) Acetonitrile. Acetonitrile is detected with poor sensitivity using NO^+; the NO^+ and H_3O^+ products are approximately equal in magnitude.

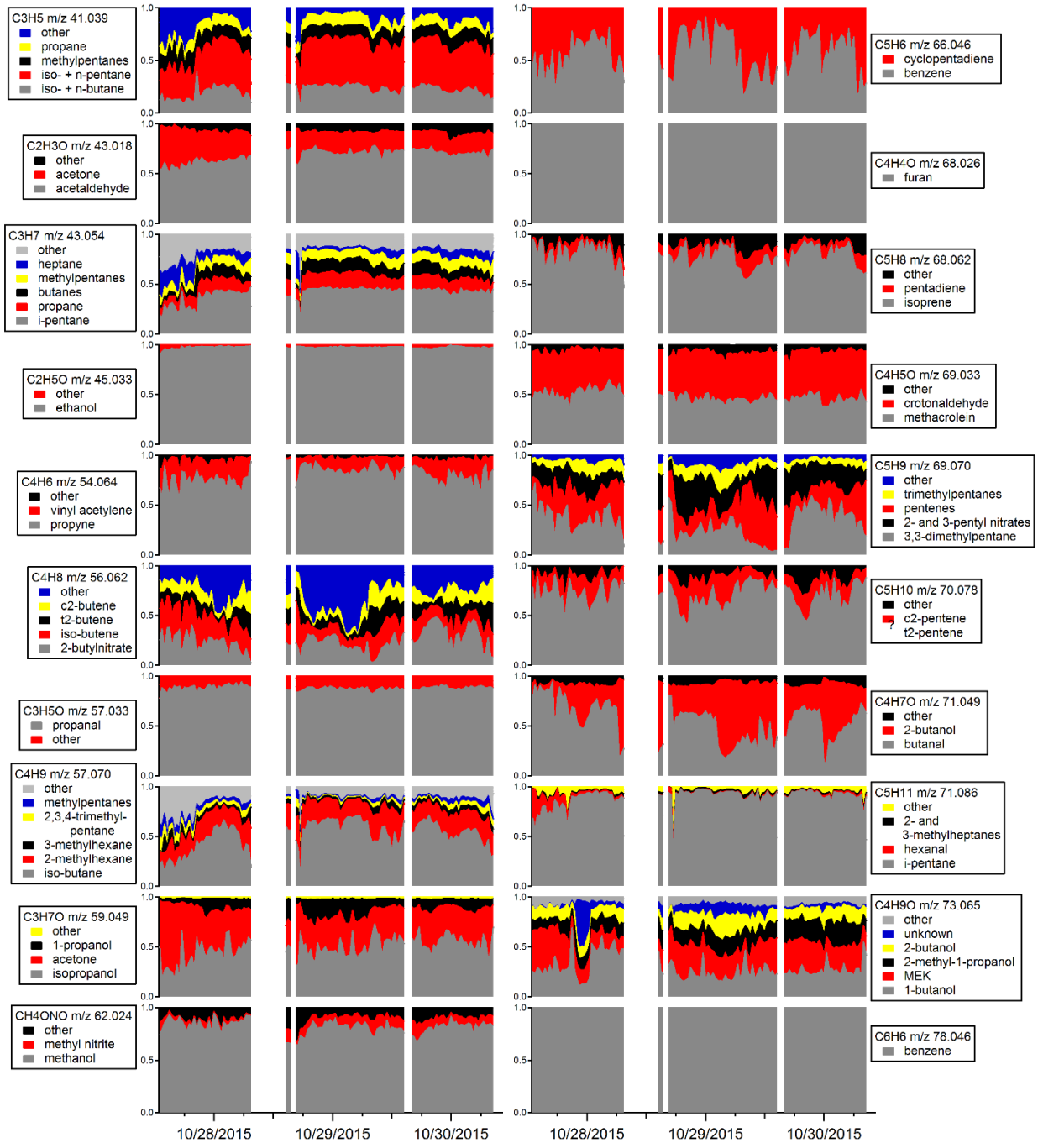

Figure S7. Speciated contributions to various NO^+ CIMS masses, in urban air. Values on Y-axes are the fractional contribution of each VOC to total signal. Includes m/z 41-m/z 78.

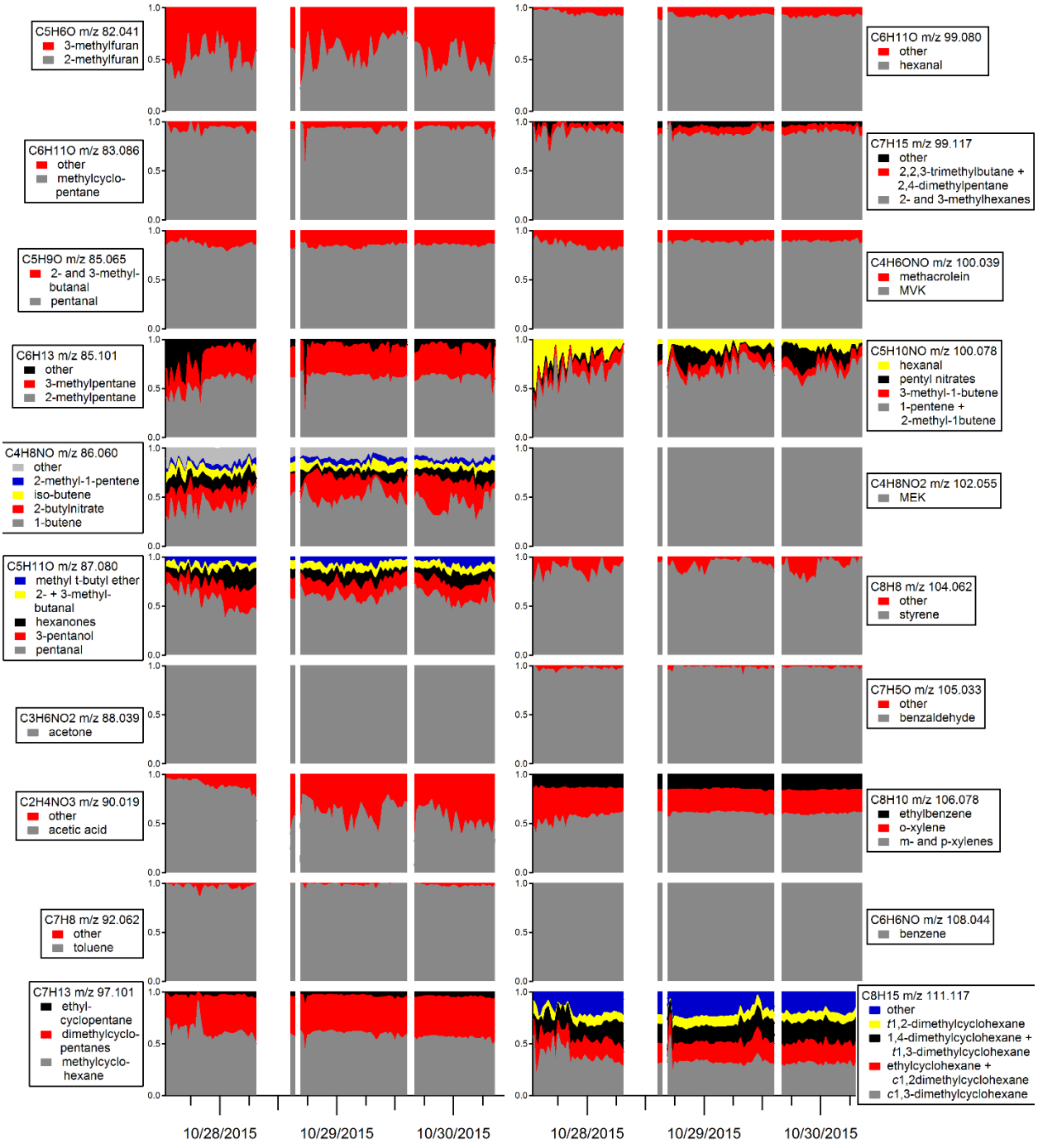

Figure S8. Figure S7, continued. Includes m/z 82-m/z 111.

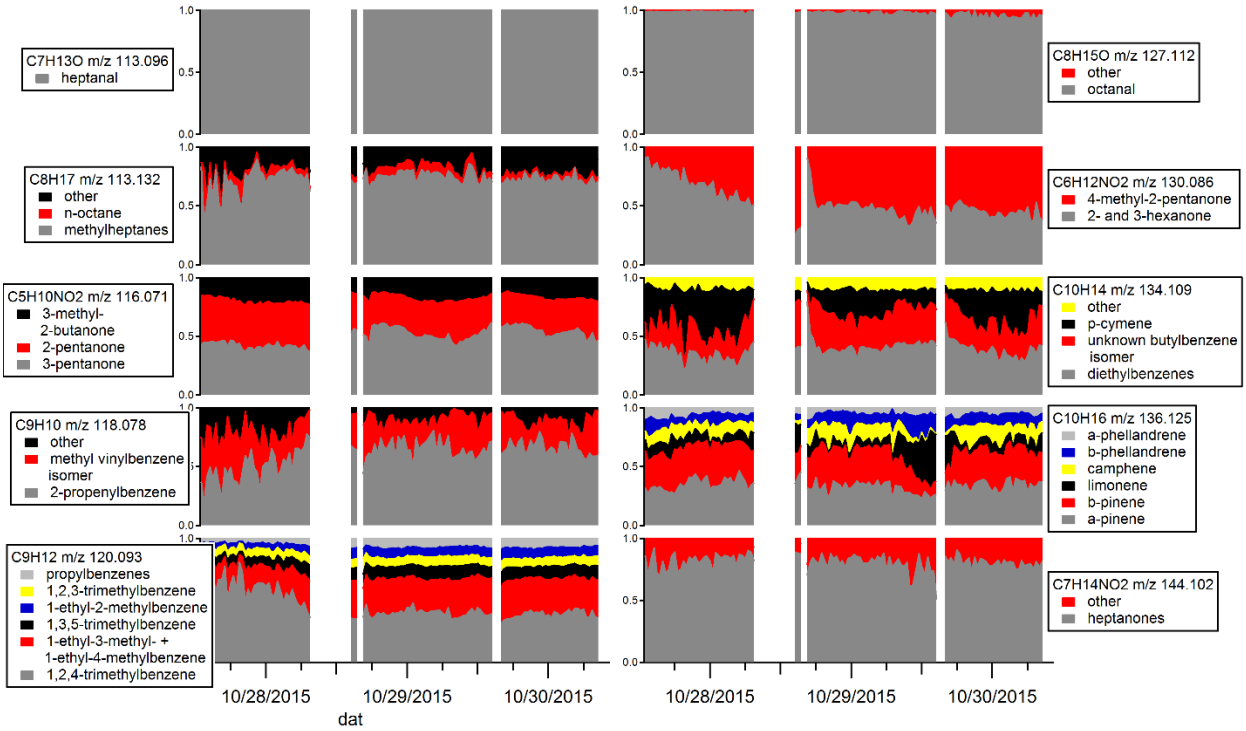

Figure S9. Figure S7, continued. Includes m/z 113-m/z 144.

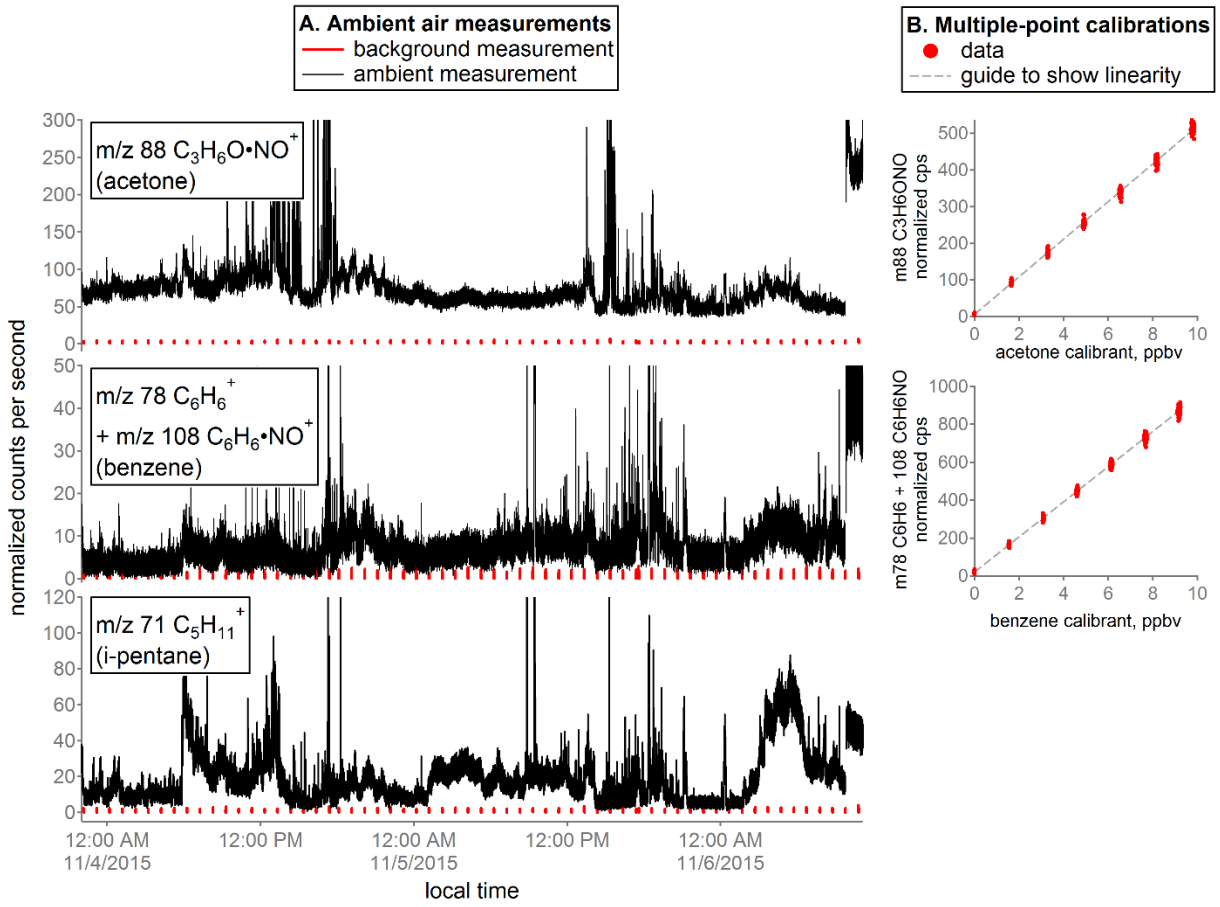

Figure S10. A. Background and ambient measurements taken during urban air sampling with the NO^+ ToF-CIMS. B. Example multiple-point calibrations of the NO^+ ToF-CIMS showing sensitivity linear with concentration.

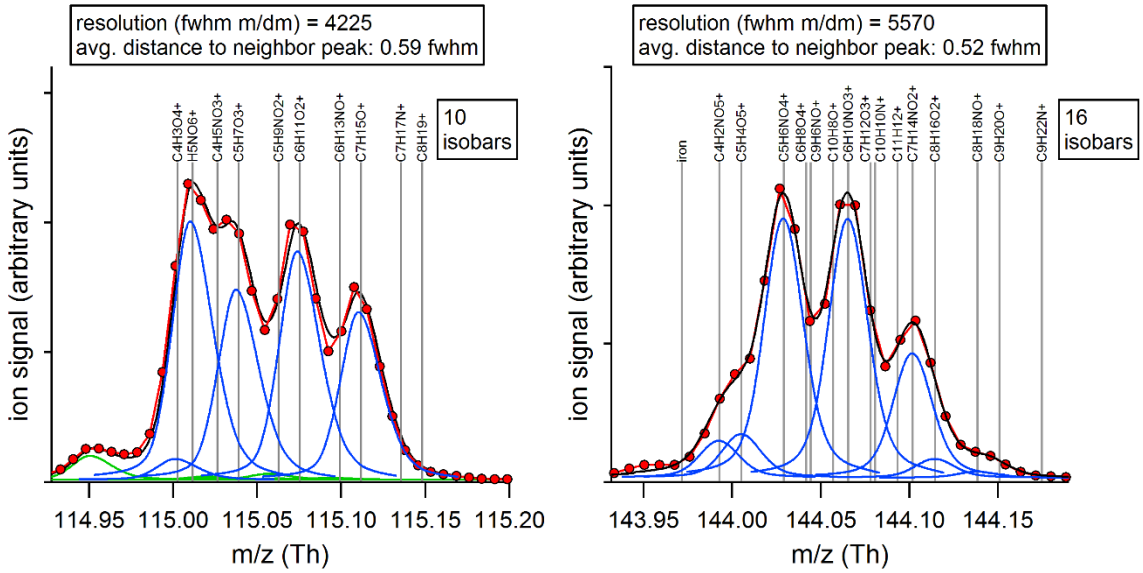

Figure S11. Example isobaric interferences for heptanone measured with H_3O^+ CIMS, at m/z 115 $C_7H_{14}OH^+$, and with NO^+ CIMS, at m/z 144 $C_7H_{14}ONO^+$. Although the resolution m/dm is better at m/z 144, there are more possible isobaric interferences and the average distance to neighboring peaks is smaller. The m/z range of each window is 10 FWHM. H_3O^+ ToF-CIMS mass spectrum courtesy of M. Coggon, collected in Boulder, CO in Dec. 2015.

Table S1. VOCs sampled in series GC-ToFCIMS laboratory experiments.

VOC name	Formula
alkanes	
ethane	C_2H_6
propane	C_3H_8
n-butane	C_4H_{10}
n-pentane	C_5H_{12}
n-hexane	C_6H_{14}
n-octane	C_8H_{18}
n-decane	$C_{10}H_{22}$
n-undecane	$C_{12}H_{26}$
i-butane (2-methylpropane)	C_4H_{10}
i-pentane (2-methylbutane)	C_5H_{12}
2,2-dimethylbutane	C_6H_{14}
2-methylpentane	C_6H_{14}
2,3-dimethylbutane	C_6H_{14}
3-methylpentane	C_6H_{14}
2,4-dimethylpentane	C_7H_{16}
2-methylhexane	C_7H_{16}
2,3-dimethylpentane	C_7H_{16}
3,3-dimethylpentane	C_7H_{16}
3-methylhexane	C_7H_{16}
2,2,4-trimethylpentane	C_8H_{18}
2,3,4-trimethylpentane	C_8H_{18}
2-methylheptane	C_8H_{18}
3-methylheptane	C_8H_{18}
4-methylheptane	C_8H_{18}
alkenes	
ethene	C_2H_4
propene	C_3H_6
ethyne	C_2H_2
trans-2-butene	C_4H_8
1-butene	C_4H_8
iso-butene (2-methylpropene)	C_4H_8
cis-2-butene	C_4H_8
1-pentene	C_5H_{10}
trans-2-pentene	C_5H_{10}
cis-2-pentene	C_5H_{10}
1-hexene	C_6H_{12}
isoprene	C_5H_8
cycloalkanes	
cyclopentane	C_5H_{10}
methylcyclopentane	C_6H_{12}
cyclohexane	C_6H_{12}
methylcyclohexane	C_7H_{14}
ethylcyclohexane	C_8H_{16}
1,1-dimethylcyclopentane	C_7H_{14}
ethylcyclopentane	C_7H_{14}
monoterpenes	
α-pinene	$C_{10}H_{16}$
β-pinene	$C_{10}H_{16}$
limonene	$C_{10}H_{16}$
camphene	$C_{10}H_{16}$
γ-terpinene	$C_{10}H_{16}$
α-phellandrene	$C_{10}H_{16}$
1,8-cineol	$C_{10}H_{16}$
3-carene + myrcene	$C_{10}H_{16}$
aromatics	
benzene	C_6H_6
toluene	C_7H_8
ethylbenzene	C_8H_{10}
m-xylene + p-xylene	C_8H_{10}
o-xylene	C_8H_{10}
vinylbenzene (styrene)	C_8H_8
isopropylbenzene	C_9H_{12}
n-propylbenzene	C_9H_{12}
1-ethyl,3-methylbenzene + 1-ethyl,4-methylbenzene	C_9H_{12}
1,3,5-trimethylbenzene	C_9H_{12}
1-ethyl,2-methylbenzene	C_9H_{12}
1,2,4-trimethylbenzene	C_9H_{12}
1,2,3-trimethylbenzene	C_9H_{12}
1,3-diethylbenzene	$C_{10}H_{14}$
1,4-diethylbenzene	$C_{10}H_{14}$
aldehydes	
acetaldehyde	C_2H_4O
propanal	C_3H_6O
butanal	C_4H_8O
pentanal	$C_5H_{10}O$
hexanal	$C_6H_{12}O$
heptanal	$C_7H_{14}O$
octanal	$C_8H_{16}O$
methacrolein	C_4H_6O
ketones	
acetone	C_3H_6O
2-butanone (MEK)	C_4H_8O
3-methyl-2-butanone	$C_5H_{10}O$
2-pentanone	$C_5H_{10}O$
3-pentanone	$C_5H_{10}O$
3-hexanone	$C_6H_{12}O$
methyl vinyl ketone (MVK)	C_4H_6O
other	
methanol	CH_4O
ethanol	C_2H_6O
2-propanol	$C3H_8O$
methyl-*t*-butyl ether (MTBE)	$C_5H_{12}O$
acetonitrile	C_2H_3N
3-methyfuran	C_5H_6O